JOURNAL OF GEOPHYSICAL RESEARCH, VOL. 101, NO. E5, PAGES 12,753–12,776, MAY 25, 1996

Mars atmospheric dynamics as simulated by the NASA Ames general circulation model, 3. Winter quasi-stationary eddies

Jeffrey R. Barnes

College of Oceanic and Atmospheric Sciences, Oregon State University, Corvallis

Robert M. Haberle and James B. Pollack[1]

NASA Ames Research Center, Moffett Field, California

Hilda Lee and James Schaeffer

Sterling Software Inc., Palo Alto, California

Abstract. A set of simulations with the NASA Ames Mars general circulation model (GCM) has been analyzed to define the basic properties and dynamics of quasi-stationary eddy circulations in the winter hemisphere. These circulations, differing substantially from those in low latitudes and the summer hemisphere, extend from the surface to the model top at ~47 km; typically, the largest geopotential and wind perturbations are found at the highest model level. Near the surface the eddies are of largest amplitude in lower latitudes, but above ~5-10 km the amplitudes are a maximum in middle and high latitudes. The vertical structure of the eddies is nearly equivalent barotropic; the phase variation in latitude is also relatively small. Zonal wavenumbers 1 and 2 dominate the stationary circulations, with wave 3 being of significance only at low levels (below ~10 km). The quasi-stationary eddies differ substantially in northern and southern winters, and undergo considerable changes with increasing dustiness in northern winter. The southern winter eddy circulation is dominated by zonal wavenumber 1, while the northern eddies have a strong wavenumber 2 component at low levels of dust loading; at high dust levels wavenumber 1 becomes dominant. This change may be at least partly the result of the dusty zonal-mean state becoming more responsive to wave 1 forcing. The standing eddies in a GCM simulation for $L_s \sim 0°$ exhibit considerable similarity in basic structure and amplitude to those revealed by a recent analysis of Viking IRTM data [*Banfield et al.*, 1996], though there are differences in the phases of the eddy patterns.

1. Introduction

One of the most striking planetary characteristics of Mars is its large topography. This topography is of the order of an atmospheric scale height, on large scales, and must have a very strong influence on the atmospheric circulation. Previous general circulation modeling of the Mars atmosphere and climate certainly has indicated that the topography is of considerable importance [*Pollack et al.*, 1981]. In addition to the topography, there are large continental-scale variations in surface albedo and thermal inertia [see *Pollack et al.*, 1990]. (In the first general circulation modeling study carried out for Mars [*Leovy and Mintz*, 1969], the albedo variations acted to force weak quasi-stationary eddies in the presence of a flat topography.) There are strong correlations of the albedo and thermal inertia variations with the topography, which could be important in the forcing of quasi-stationary circulations [*Zurek et al.*, 1992].

At present, there are very limited observational data that could reveal the presence of quasi-stationary eddy circulations in the Martian atmosphere. This is a consequence of the nature of the data, which have been obtained by spacecraft in relatively long-period (~1 day) orbits with moving nadir longitudes, and by two isolated surface stations. Future data to be obtained by atmospheric sounders on spacecrafts in short-period, polar orbits (such as the Thermal emission spectrometer (TES) and Pressure modulator infrared radiometer (PMIRR) instruments) will allow a determination of the basic structure of the quasi-stationary eddies.

Despite the shortcomings of the current data sets, they do provide evidence for the existence of planetary-scale, quasi-stationary eddies. In particular, recent analyses of the Viking infrared thermal mapper (IRTM) 15-μm data have revealed the

[1]Deceased, June 13, 1994.

Paper number 96JE00179.
0148-0227/96/96JE-00179$09.00

presence of such eddies in both hemispheres during a time period centered on $L_S \sim 0°$ [*Banfield et al.*, 1996]. These eddies exhibit a predominantly wavenumber 2 pattern in the northern hemisphere and a wavenumber 1 pattern in the southern hemisphere, with the temperature amplitudes being of the order of 1-2 K. The Mariner 9 infrared imaging spectrometer (IRIS) data previously yielded evidence for planetary-scale disturbances in late northern winter, which could have been stationary or nearly stationary [*Conrath*, 1981]. The temperature amplitude of these disturbances exhibited a maximum of ~4 K at relatively high levels, ~20-30 km, in middle and high northern latitudes. The Viking IRTM data set also contains evidence for planetary-scale disturbances at the 20 to 30-km levels during the 1977 northern winter solstice global dust storm, with the 15-μm temperatures indicating the possible presence of a nearly stationary zonal wavenumber 1 circulation [*Murphy et al.*, 1995] in northern middle and high latitudes. The nature of the Viking orbits gives such a feature a roughly 13-day periodicity in the IRTM observations [*Jakosky and Martin*, 1987; *Murphy et al.*, 1995]. The coincidence of this disturbance with the global dust storm and a north polar warming [*Martin and Kieffer*, 1979] certainly is suggestive that it may have been involved in producing the latter event.

A possible source of evidence for the existence of stationary eddy circulations in the Martian atmosphere is the collection of observations (images) of surface features produced by winds. The primary difficulty with this set of data, though, is the limited knowledge of exactly when and how the various features form: in particular, to what extent do these features represent average winds as opposed to peak winds at particular times? Most of the surface streak data are at relatively lower latitudes, and the distribution of bright streaks in this region seems to largely reflect the low-level flow in the Hadley cell near northern winter solstice [*Greeley et al.*, 1993]. Some of the bright streaks in the middle and higher latitudes may provide information about the standing eddy circulations, but again, it is difficult to assess which streaks are truly indicative of the larger-scale flow during the winter season. Many of the midlatitude streaks in the maps by *Greeley et al.* [1993] appear likely to have been produced either by smaller-scale winds (e.g., slope flows) or by winds at other seasons.

A number of theoretical and modeling studies of quasi-stationary eddies in the Martian atmosphere have previously been carried out. These include the earlier global circulation model (GCM) studies referred to above, and several studies performed using simplified models. *Mass and Sagan* [1976] employed a two-level, quasi-geostrophic model and found large, quasi-stationary circulations in southern winter associated with the prominent Tharsis and Hellas topographic features. *Gadian* [1978] utilized a linear (multilevel) quasi-geostrophic model to examine forced stationary eddies, finding that planetary-scale eddies could achieve large amplitudes at high levels. A linearized (two-level) primitive equation model was used by *Webster* [1977] to investigate the effects of mechanical and thermal forcing associated with large topography in low latitudes. Webster obtained large-amplitude atmospheric responses in both the tropics and the winter extratropics, with the thermal forcing appearing to be quite important. Recently, *Hollingsworth and Barnes* [1996] conducted a linear study focusing upon the winter extratropical atmosphere. Some of the results from this investigation are of considerable interest in relation to the quasi-stationary eddies in the current set of GCM simulations, and these are noted in the context of the GCM results presented in the following sections of this paper.

The quasi-stationary eddies in the GCM experiments differ greatly between the winter extratropics and the tropics and the summer hemisphere; this was also found to be the case in the earlier GCM studies [*Pollack et al.*, 1981]. In part, this reflects the great differences in the mean states in these different regions [see *Haberle et al.*, 1993]. The zonal-mean zonal winds in the winter extratropics are westerly, with a very strong circumpolar jet in middle and high latitudes. This westerly flow allows the vertical penetration of planetary waves, up to the highest model levels. In contrast, there are mostly easterly winds in the tropics and the summer hemisphere, and these vertically trap the quasi-stationary eddies. An additional factor of considerable importance is the very strong cross-equatorial Hadley circulation that exists near the solstices [see *Haberle et al.*, 1993]. The lower branch of this cell is most intense in the tropics and the summer hemisphere, and its interaction with topography gives rise to very strong regional asymmetries in the time-mean flow. These have been referred to as western boundary currents in recent studies based upon a simplified GCM [*Joshi et al.*, 1994, 1995]. There is also a strong low-level westerly jet in the southern summer subtropics associated with the Hadley cell [*Haberle et al.*, 1993], and this appears to play a large role in forcing time-mean eddy circulations in the summer southern hemisphere. In view of the considerable differences in the structure and dynamics of the quasi-stationary eddies in the winter extratropics, and the tropics and the summer hemisphere, this paper focuses upon the former region only.

Section 2 gives a brief summary of the current NASA Ames Mars GCM and the set of simulations analyzed in this study. This is followed by sections presenting aspects of the basic structure and the dynamics of the quasi-stationary eddies in these simulations. The final section briefly summarizes and discusses the results of this investigation.

2. The GCM Simulations

The model used to produce the simulations examined in this paper is an improved version of the NASA Ames Mars GCM [*Pollack et al.*, 1981]. *Pollack et al.* [1990] gave a detailed description of this version, and *Barnes et al.* [1993] and *Haberle et al.* [1993] provided discussion of some of the aspects of the model that are of greatest significance for dynamical processes. Very briefly, the Mars GCM is a finite difference model in sigma coordinates which was originally adapted from an Earth GCM. All the simulations analyzed in this study were run with 13 vertical layers and the (dynamical) top of the model at a height of 45-50 km. The horizontal resolution in the simulations was 7.5° latitude × 9° longitude. It does not appear (on the basis of a sensitivity experiment with a higher resolution) that this resolution has any major impact on the eddy circulations examined here, as these are of planetary scale.

All of the simulations examined in this study are "static dust" experiments, in which the atmospheric dust is not transported by the circulation (but does impact the radiative forcing). The horizontal dust distribution (the vertical dust opacity) is uniform except for the effects of topography, and the vertical profile of the dust mixing ratio is nearly uniform

in the lower atmosphere with a falloff at higher levels [see *Pollack et al.*, 1990].

The variable surface fields of topography, thermal inertia, and albedo incorporated in the GCM are responsible for forcing the quasi-stationary eddies. For the basic set of experiments, these fields were derived from Mars Consortium data sets [see *Pollack et al.*, 1990; *Hollingsworth and Barnes*, 1996]. In addition, several experiments have been performed with a topography that is based upon the more recent Mars digital terrain model (DTM) data set [*Wu et al.*, 1986]. All of the surface fields were smoothed to the resolution of the Mars GCM.

The topography employed in most of the experiments is shown in Figure 1. Major features are the huge Tharsis "bulge" between 60° and 120° W, which extends well into both hemispheres, the Arabia and Noachis Terra uplands near 60° E, the elevated Elysium region near 150° E in the north, and the Hellas basin near 80° E in the southern hemisphere. The topography at high latitudes in both hemispheres is relatively smooth (it is actually completely flat poleward of 75° S due to a lack of data in the Consortium model), but there is a very prominent zonally symmetric depression centered at ~65° in the northern hemisphere. The DTM topography is basically similar to the Consortium topography in most respects, except that the south polar region is quite elevated (~4-5 km). Although there are very sizeable (~1-2 km) local differences in the two topographies (reflecting the absolute uncertainties in the data), the planetary-scale variations in the relative heights are less different.

The current version of the Mars GCM incorporates a Rayleigh friction "sponge layer" near the model top to help minimize problems associated with wave reflection from the upper boundary [*Pollack et al.*, 1990]. A sensitivity experiment was performed to examine the effects of this dissipation (which has a minimum timescale of 2 days), and it does not appear to have any substantial effects upon the stationary eddies. The GCM does not incorporate any explicit diffusion but does employ a longitudinal smoothing at high latitudes to minimize problems with linear computational instability.

The set of GCM simulations examined in this study spans a broad range of seasonal dates and dust loadings (many of the experiments are listed in Table 1 of *Haberle et al.*, [1993]. In all the simulations the model is started up from rest and run with a continuously varying seasonal date. Most of the experiments examined in this study are 50 days in length, with the last 30 days of data used for analysis. The history data for the 30-day periods are saved at intervals of 1.5 hours (16 points per Mars day). Most of the results presented here represent averages of these model data over the 30-day periods, this averaging removing the signals of transient disturbances (such as baroclinic eddies and thermal tides). In most cases, the model data have been interpolated to constant pressure surfaces before being analyzed.

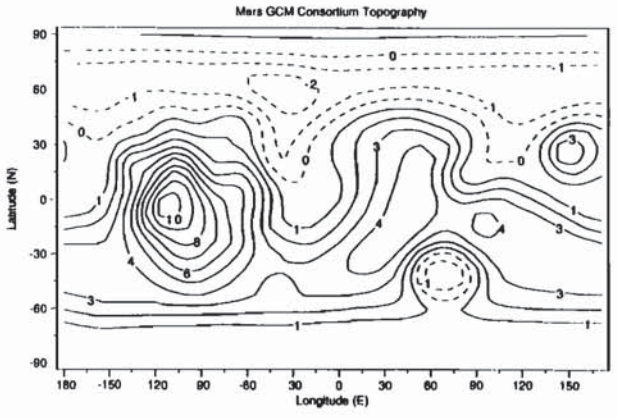

Figure 1. The smoothed Mars Consortium topography used for most of the GCM simulations. Poleward of about 70° in the south the topography is completely flat because of an absence of data.

3. Eddy Structure

In this section the structure of the winter quasi-stationary eddies in the GCM simulations is discussed. In light of the uncertainties in the topography used in the current version of the GCM, the focus is on the more essential aspects of the eddy structure, which are found to be quite similar in simulations performed with both of the available topography data sets.

3.1. Northern Hemisphere Winter

Figure 2 shows several aspects of the structure of the quasi-stationary eddies in a simulation for northern winter solstice and a relatively low dust loading (optical depth 0.3). It can be seen that the eddies exhibit sizeable amplitudes at both lower and upper atmospheric levels, though the upper level amplitudes are larger. The eddy structure appears to be quite (equivalent) barotropic, with the upper level structure being aligned quite closely with that at lower altitudes. It can be noted that the upper level disturbances are located somewhat further poleward than those at the lower level. The longitudinal structure of the eddy circulations corresponds to a zonal wavenumber 2 pattern in the eastern hemisphere, with only a very weak circulation being present in the western hemisphere. It can be noted that the locations of the ridges and troughs at the lower level are close to the locations of the topographic maxima and minima in middle latitudes (see Figure 1).

The barotropic nature of the eddy structure is further illustrated in Figure 3, in the form of a longitude slice at 60° N. Some vertical phase tilt is apparent, especially in the ridge between ~0 and 60° E, but this tilt is small: there is less than one-quarter wavelength of phase change between the surface and the model top at ~47 km. It can be seen in Figure 3 that the maximum amplitudes are reached at or near the model top. At lower latitudes, the maximum amplitudes are found at lower levels, reflecting a northward shift of the maximum eddy amplitude with height.

Figure 4 shows several aspects of the latitude-height structure of the winter eddies, illustrating the northward shift of the maximum amplitudes with increasing altitude. There are low-level maxima in both the temperature and kinetic energy fields located in the tropics, with the rms geopotential height having a secondary maximum in this region. The large eddy amplitudes at low latitudes near the surface are certainly suggestive as to the importance of forcing by the very large topography in the tropical region. There is a secondary maximum in the temperature amplitude at middle atmospheric

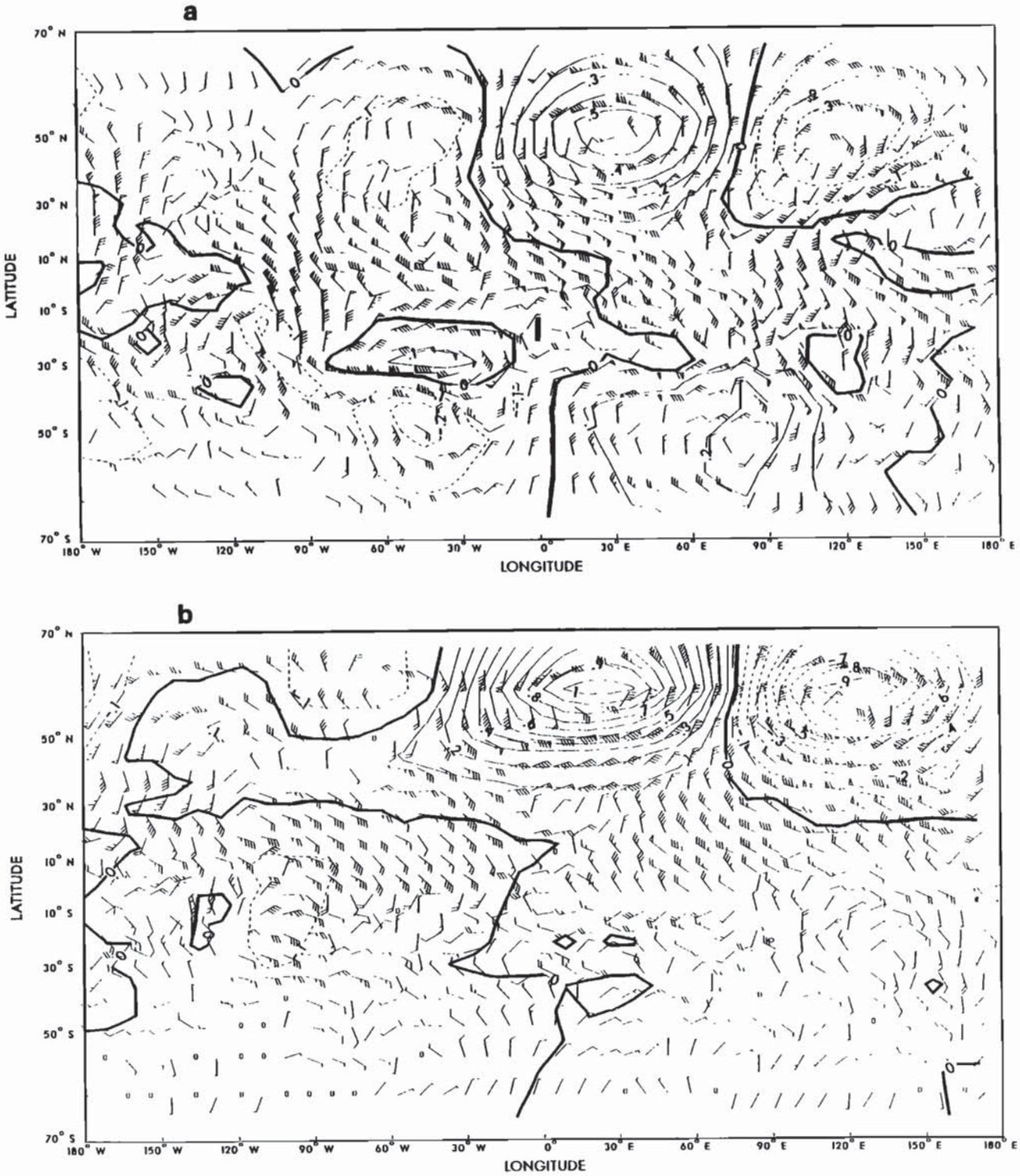

Figure 2. Time-averaged eddy geopotential height (in kilometers) and winds from a northern winter solstice simulation with an optical depth of 0.3, at the (a) 3-mbar level, and the (b) 0.3-mbar level. On the wind arrows, a flag represents 10 m/s, while barbs and half-barbs denote 2 m/s and 1 m/s.

levels, with the other two fields exhibiting maxima at or near the model top. It can be noted that the height of the secondary temperature maximum is quite similar to that characterizing the Mariner 9 IRIS eddies [*Conrath*, 1981].

Large eddy amplitudes are present at lower levels in the southern hemisphere in Figure 4. These are associated with the strong westerly subtropical jet interacting with the large topography in the southern hemisphere, as well as with the effects of thermal forcing in the summer hemisphere.

The horizontal heat and momentum fluxes associated with the winter eddies are shown in Figure 5. It can be seen that these eddies are basically transporting heat and

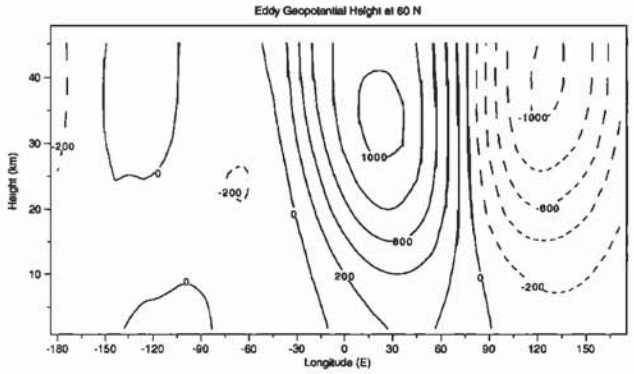

Figure 3. A cross section of eddy geopotential height (in meters) at 60° N, from the same simulation as in Figure 2. The heights on the vertical axis are averages for the data pressure levels in the GCM.

momentum poleward, though there are equatorward fluxes at lower levels and in lower latitudes. The (weak) westward phase tilt apparent in Figure 3 is consistent with the northward heat fluxes and implies an upward energy propagation, to the extent that group velocity considerations can be meaningfully applied to the eddy circulations. The poleward momentum fluxes imply an equatorward propagation. The smallness of both fluxes is noteworthy, though, as the magnitudes of the products of the wind and temperature amplitudes (see Figure 4) are much larger. This reflects the small phase tilts in both height and latitude, which result in very small correlations between the eddy quantities (within the context of quasi-geostrophic dynamics, the heat and momentum fluxes are directly proportional to the vertical and meridional phase tilts [see *Andrews et al.*, 1987]). The stationary eddy heat and momentum fluxes are relatively small (less than half as large) in comparison to the transient eddy fluxes [see *Barnes et al.*, 1993, Figure 27].

Figure 6 shows the horizontal eddy structure at a middle level (the structure is very equivalent barotropic) for a northern winter solstice experiment with an optical depth of 1. It can be seen that the structure resembles that in Figure 2, but there is a much stronger ridge and trough pair in the western hemisphere. In other basic respects the structure is very similar to that in the simulation with the smaller dust loading, though the eddy amplitudes are slightly larger. As will be discussed below, much larger amplitude eddy circulations are present in this moderately dusty solstice simulation, but these are slowly propagating and changing in time, and they do not show up in the full 30-day time average.

Also shown in Figure 6 is the eddy temperature field at the lowest GCM sigma level (at a height of ~250 m). This illustrates the existence of large low-level eddy amplitudes extending into the subtropics and the tropics in northern winter (as can be seen in Figure 4). The equivalent barotropic nature of the eddies is apparent in Figure 6, with warm regions largely coinciding with elevated areas and cold regions with low-lying areas (see Figure 1). The relatively narrow cold "tongue" located at ~30°-50° W in Figure 6, with a temperature minimum at ~5°-10° N, is associated with a regional intensification of the equatorward Hadley flow on the eastern flanks of the Tharsis uplands: a western boundary current similar to flow structures found in a simplified GCM [*Joshi et al.*, 1994, 1995]. It can be noted that the eddy thermal structure in Figure 6 will tend to produce local enhancements in the prevailing north-south temperature gradient in the regions of the uplands, and decreases in this gradient in the lowland areas. Analyses of the transient eddy activity in the GCM simulations reveal that there are large regional variations (in midlatitudes), and these appear to be linked to the regional differences in the low-level baroclinicity [*J. L. Hollingsworth et al.*, 1996].

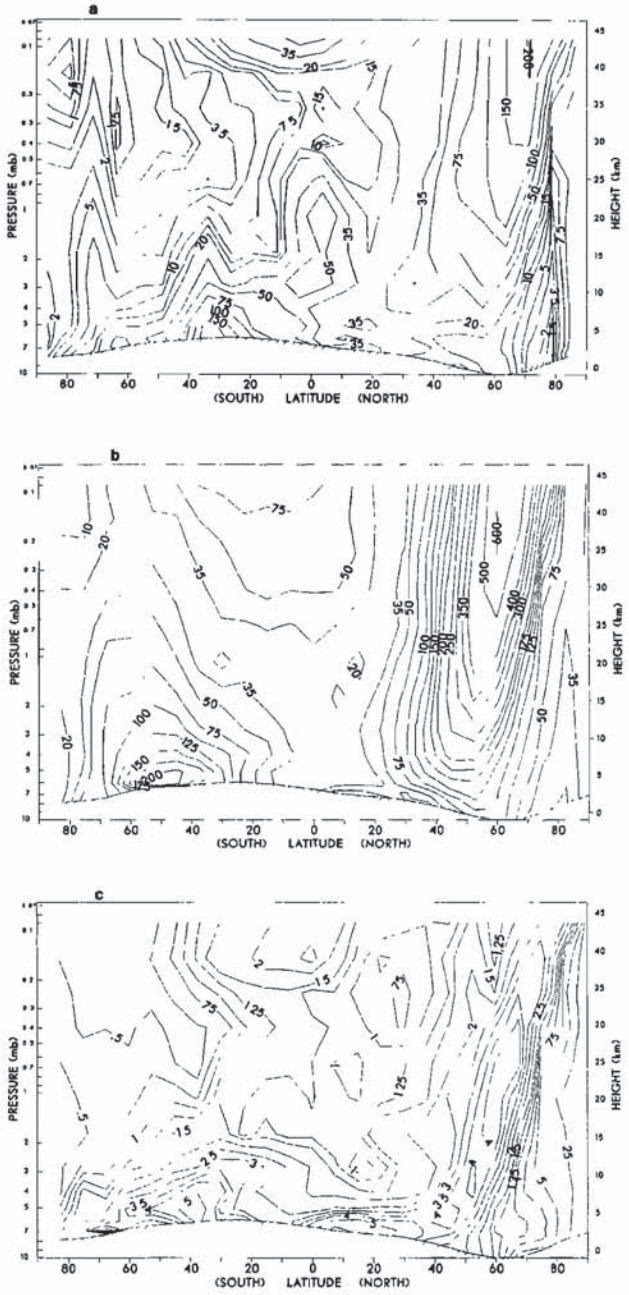

Figure 4. Latitude-height cross sections of several measures of the stationary eddy amplitudes, from the same simulation as in Figure 2: (a) the eddy kinetic energy density (in m^2s^2) (b) the rms height variance (m^2), and (c) the rms temperature variance (in Kelvins).

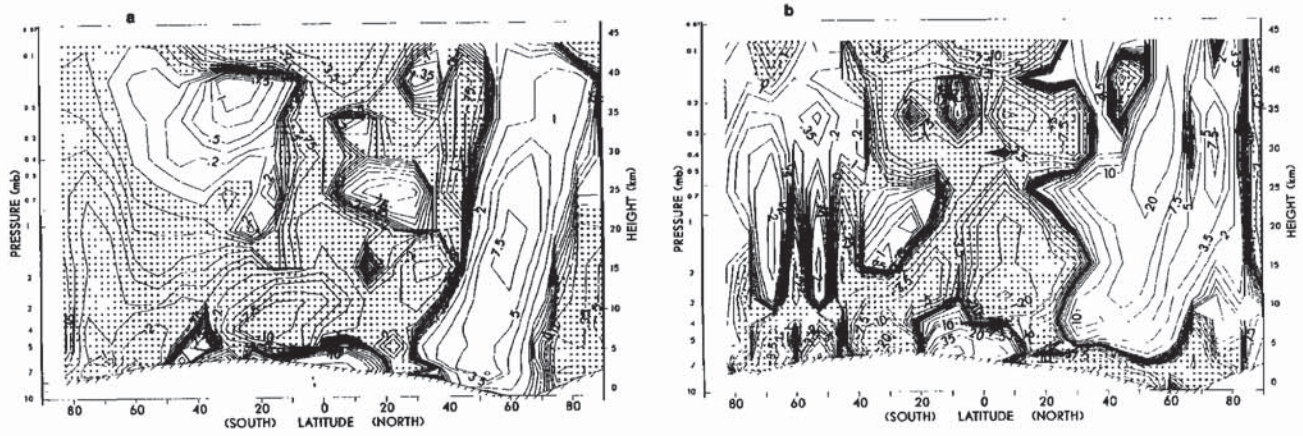

Figure 5. Latitude-height cross sections of (a) the stationary eddy meridional heat flux (values in K m/s) and (b) the stationary eddy meridional momentum flux (values in m^2s^2), from the simulation in Figure 2.

The horizontal eddy structure from the same experiment, but with the DTM topography used in place of the Mars Consortium topography, is shown in Figure 7. It can be seen that the basic structure is quite similar in the two cases, but the eddy amplitudes are substantially larger in the DTM simulation. In the DTM experiment there are large eddy amplitudes in the tropics at low levels, as with the Consortium topography, and the wind and geopotential amplitudes peak at the model top. It can be noted that the zonal-mean flows in the two simulations are very similar, so that the differences in the stationary eddies in the two cases must largely reflect the topographic differences (the thermal inertia and albedo fields are identical). In this regard, it is significant that the amplitudes of the zonal wavenumber 1-3 topographic components are all larger in middle latitudes in the DTM case than for the Consortium data. In the 40°-50° N region, the amplitude of wavenumber 2 is roughly double that for the Consortium topography. To the extent that the DTM topography is a more accurate representation of Mars than the Consortium version, then the quasi-stationary eddy

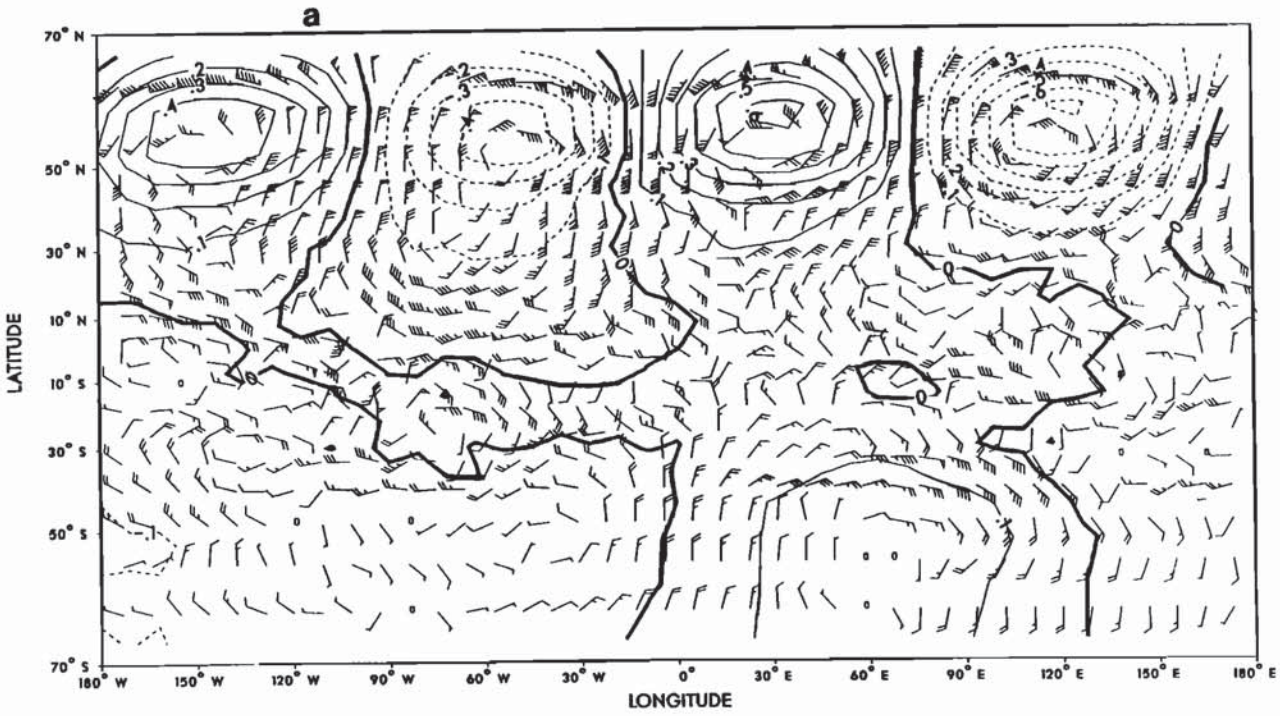

Figure 6. (a) Eddy geopotential and wind structure (as in Figure 2) at the 1-mbar level for a simulation for northern winter solstice and a dust optical depth of 1, along with (b) the eddy temperature field at the lowest GCM sigma level (at a height of ~250 m).

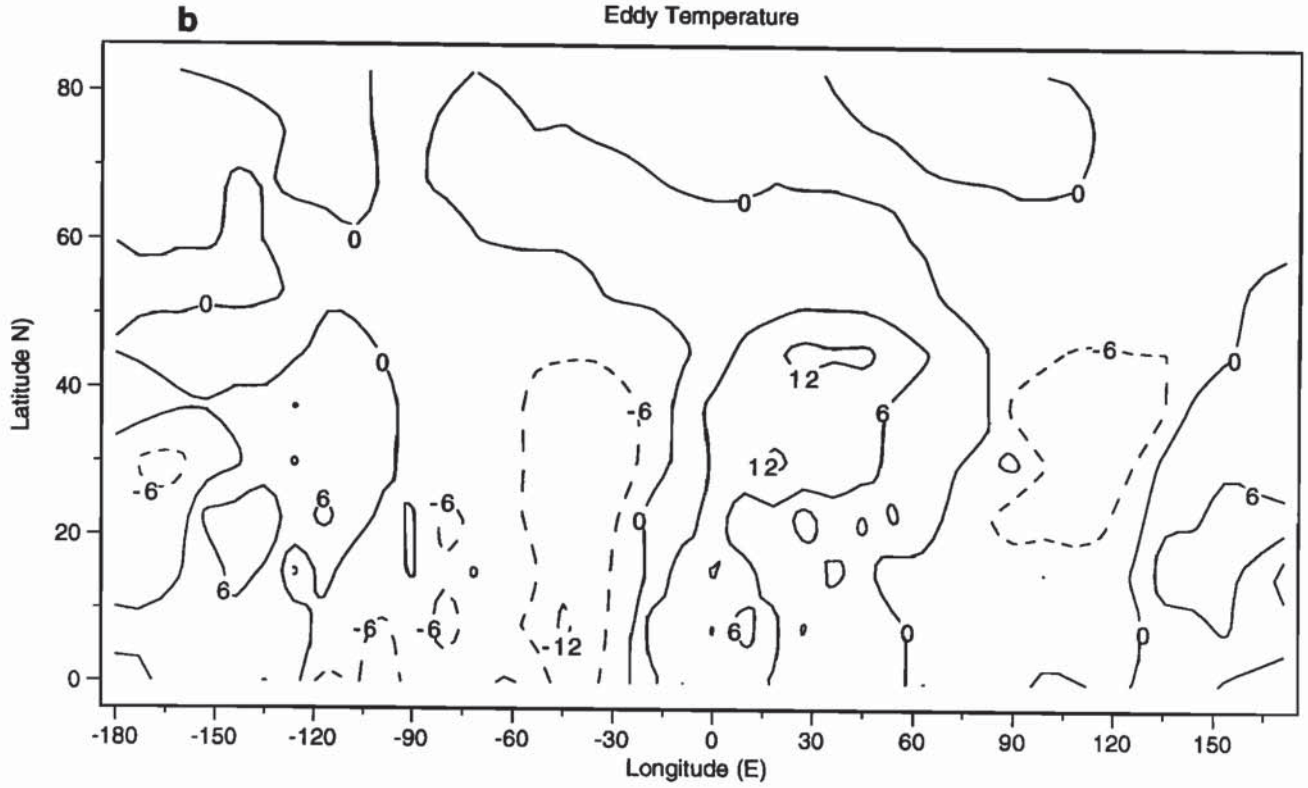

Figure 6. (continued)

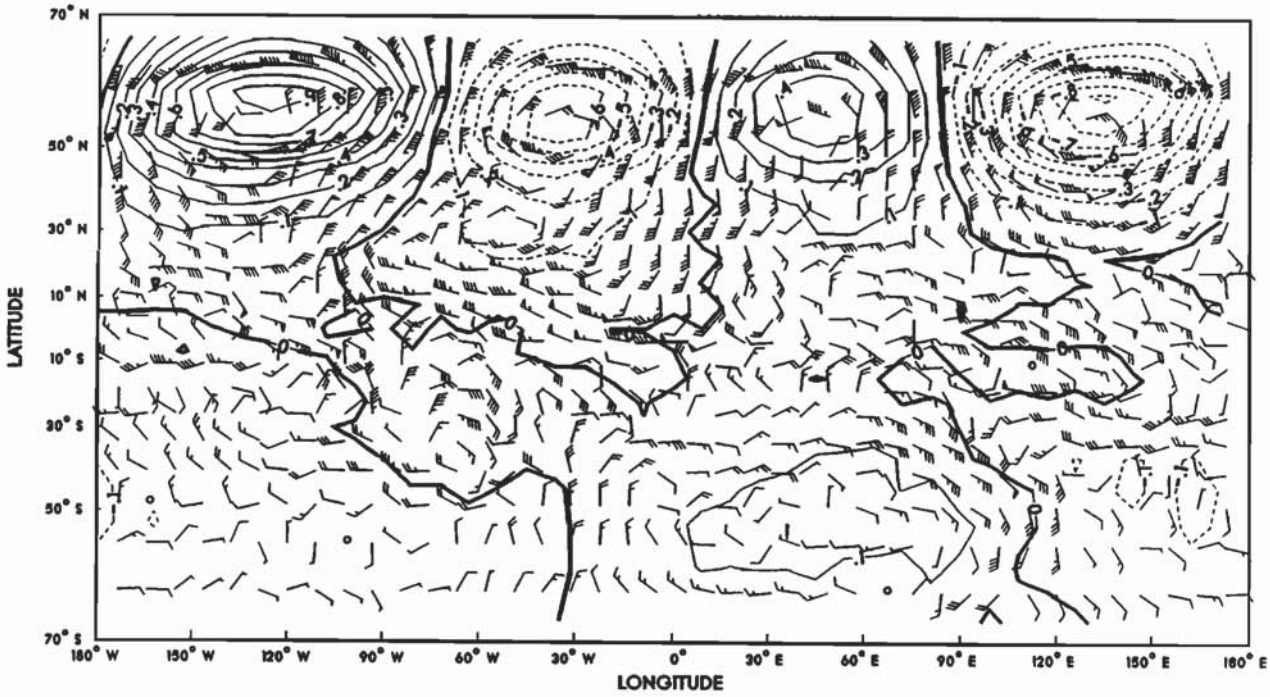

Figure 7. As in Figure 6, but for a GCM simulation with the DTM topographic data set.

circulations in northern winter may be expected to be more vigorous than they are in the GCM experiments with the Consortium data.

3.2. Southern Hemisphere Winter

Figure 8 shows the horizontal eddy structure at a lower and an upper level from a simulation for southern winter solstice (for a dust opacity of 0.3). The striking feature is the very large amplitude zonal wavenumber 1 pattern which is present at the higher level. The wavenumber 1 pattern is also apparent at the lower level, though significant wavenumber 2 and 3 components are also present (the wave 3 component is actually largest). A very interesting aspect of the wave 1 structure is that the pressure ridge is located between ~70° and 140° west of the wave 1 topographic ridge in middle latitudes and the subtropics (which is in the Tharsis region). In contrast, the wave 2 and 3 components of the stationary flow

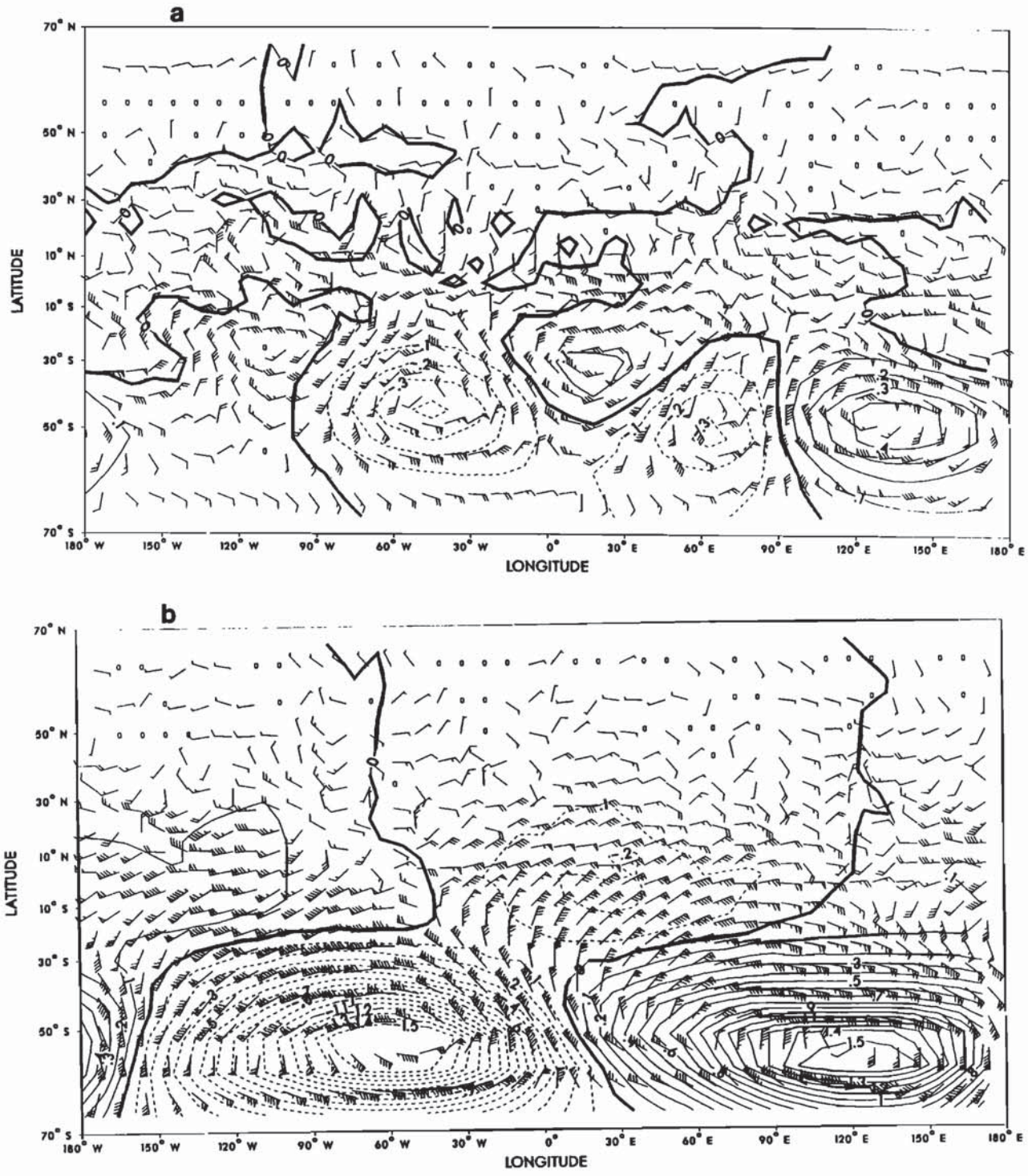

Figure 8. As in Figure 2, but for a simulation for southern winter solstice with an optical depth of 0.3.

are both nearly in phase with the corresponding topographic components.

Aspects of the latitude-height structure for the southern winter experiment are shown in Figure 9. It can be seen that the patterns are qualitatively similar to those for the northern winter case, but the maximum lower level amplitudes are located at somewhat higher latitudes, namely, in the subtropics and midlatitudes, instead of the tropics. In this regard, it can be noted that there are quite large planetary wave amplitudes (in excess of 1.5 km) for the southern hemisphere

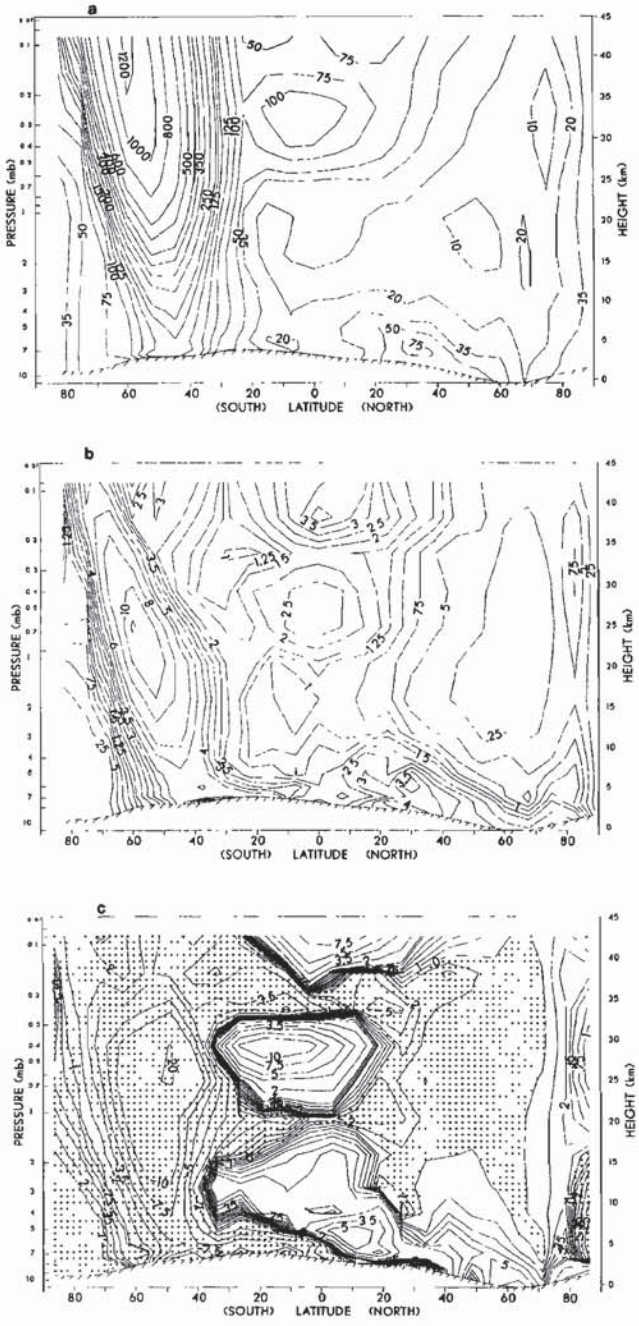

Figure 9. Latitude-height cross sections of eddy structure for the southern winter case in Figure 8: (a) the rms height, (b) the rms temperature, and (c) the eddy meridional heat flux. The units are as in Figure 4.

topography in the vicinity of 40° S [see *Hollingsworth and Barnes*, 1996]. It appears that forcing by the large topography in the tropics is distinctly less important for the southern eddies than for those in northern winter.

The horizontal heat transport for the southern winter simulation, (Figure 9), is characterized by much larger poleward fluxes than the northern winter case (see Figure 5). The peak fluxes, both at the surface and aloft, are roughly 3 times as large as in the northern winter simulation; these fluxes are greatly in excess of the transient eddy heat fluxes in the southern winter experiment (these are quite small, in line with the low level of transient eddy activity at this season [see *Barnes et al.*, 1993]). For the southern winter solstice circulation in the Mars GCM, then, the quasi-stationary eddies are dominant in the eddy heat transport process, whereas the transient eddies are of greater importance at northern winter solstice. The latter also appear to play a more important role in producing dust transports in recent northern winter simulations performed with a version of the Mars GCM that is coupled with an aerosol transport model [*Murphy et al.*, 1995].

The results from an experiment for southern winter solstice with the DTM topography (not shown) are very similar to those shown in Figure 9 for the Consortium topography. The amplitudes are somewhat larger, though not nearly as much so as in the northern winter DTM case.

Sensitivity experiments performed with hemispherically reversed (Consortium) topographies (the southern hemisphere topography placed at northern latitudes and vice versa) show directly that the large differences in the topographies in the two hemispheres are primarily responsible for the differences in the quasi-stationary eddies in the southern and northern winter seasons. The differences in the seasonal thermal forcing and zonal-mean states must play a rather secondary role, since the hemispherically reversed topography simulations yield standing eddy patterns which are quite similar to those presented above, for the winter solstice seasons in the opposite hemispheres.

3.3. Changes in Dust Loading and Season

The horizontal eddy structure at a lower level is shown in Figure 10, for a simulation for northern winter solstice with a dust opacity of 2.5. Though the pattern at the lower level (not shown) is somewhat similar to that in Figure 2 for an opacity of 0.3, the upper level pattern can be seen to be very different. A strong wavenumber 1 disturbance is clearly present at the higher level; this pattern also dominates at the 1-mbar level (not shown). The amplitudes of the quasi-stationary eddies in this dusty experiment are substantially larger than in the relatively nondusty case, being somewhat larger also than those of the transient eddies. The poleward eddy heat fluxes, shown in Figure 11, are substantially greater than in the nondusty simulation, and are evidence of strong low-level circulations in the tropics which appear to extend into middle latitudes. In the dusty experiment the stationary eddy heat fluxes are comparable in magnitude (larger near the surface) to the transient fluxes.

The relative phase of the wavenumber 1 pattern (in geopotential) apparent in Figure 10 is of interest, in that it differs significantly from the phase of the wavenumber 1 component present in the nondusty simulation. In particular, the position of the high is ~60°-90° further east in the dusty

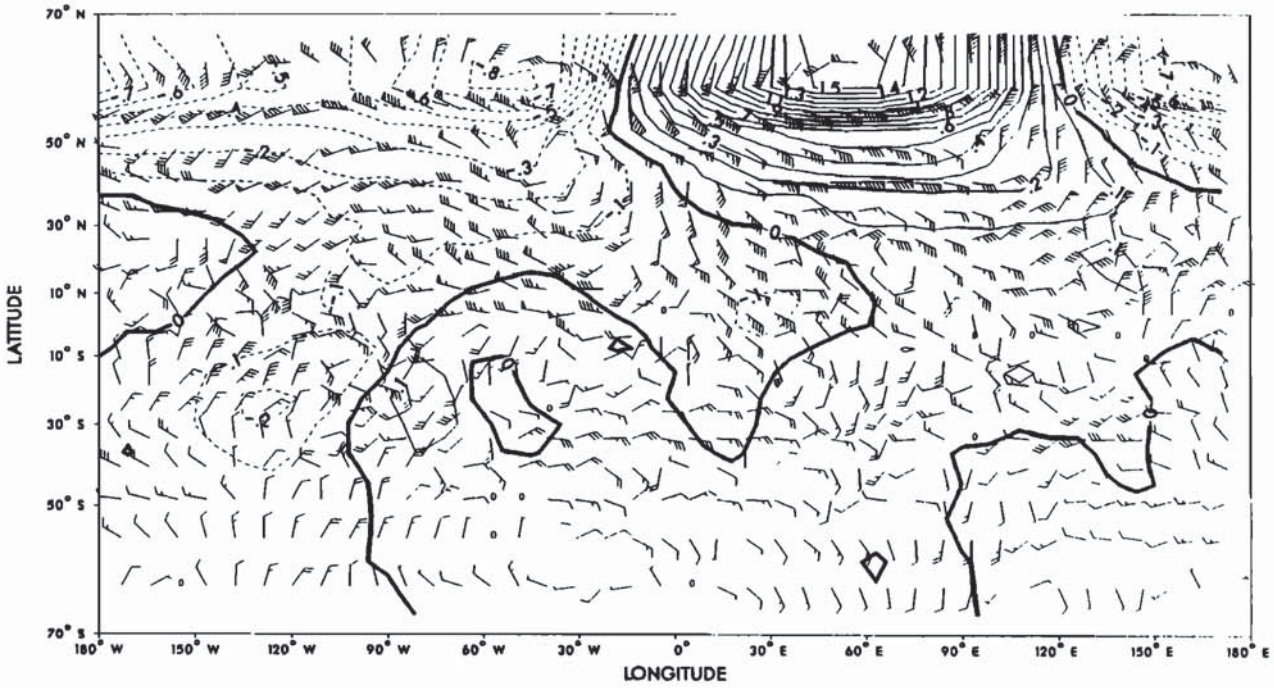

Figure 10. The eddy geopotential heights and temperatures (as in Figure 2) at the 0.3-mbar level, for a northern winter solstice simulation with a dust opacity of 2.5.

case, being located at ~50°-60° E (the lower and upper levels are separated by only about 10 degrees of phase). This is in the vicinity of the position of the wavenumber one topographic ridge in midlatitudes. In contrast, the wavenumber 2 and 3 geopotential components in the dusty simulation have phases which are very similar to those in the nondusty case, phases very similar to those of the topographic components.

At an even higher dust loading (an optical depth of 5), the northern winter quasi-stationary eddies in the Mars GCM are similar to those in the 2.5 opacity simulation. However, their amplitudes and fluxes are somewhat smaller in the extremely dusty experiment.

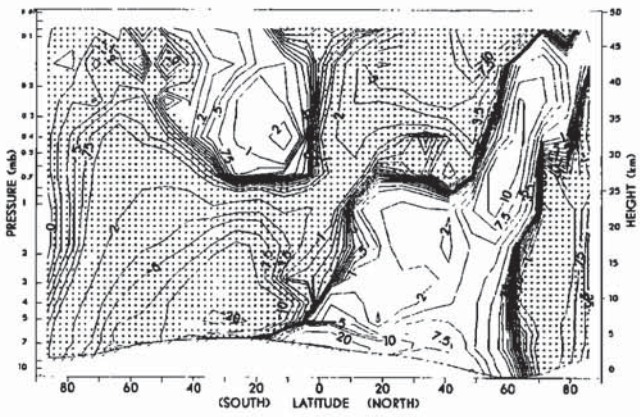

Figure 11. The eddy meridional heat flux (units as in Figure 4) for the dusty simulation in Figure 10.

There are stationary eddies present in GCM simulations for both early northern autumn and late northern winter seasons (with low to moderate dust loadings). The basic structure of these eddies is rather similar in both cases, and is not very different from that at winter solstice. The horizontal structure is dominated by a wavenumber 2 pattern, at lower and upper levels. Figure 12 shows the late winter structure at the 1-mbar level. The amplitudes and fluxes of the early fall and late winter eddies are reduced by comparison with the solstice case, though the geopotential and wind amplitudes still reach their maximum values at the top of the model.

Also shown in Figure 12 is the temperature field at the 0.65-mbar level from a GCM experiment (30 days of data) centered at $L_S \sim 0°$ (with a dust optical depth of 0.3). This can be compared with the results obtained by *Banfield et al.*, [1996] from Viking IRTM 15-μm data for a 112-day period centered at this same seasonal date. The GCM results exhibit the same basic predominantly wavenumber 2 structure in the northern hemisphere and wavenumber 1 pattern in the southern hemisphere as the observational data, and the magnitudes of the temperature perturbations in the GCM are very similar to those in the data (~1-2 K). There are some differences in the locations of the warm and cold regions, however. The wavenumber 1 pattern in the south is shifted further to the west in the observations (by ~90 degrees of longitude, or one-quarter wavelength), as is the wave 2 field in the north. The comparison with the IRTM data is not a direct one, certainly, since the averaging period used by *Banfield et al.* covers a much greater range of L_S than that covered in the GCM simulation. The standing eddies in the GCM undergo considerable changes during the period spanned by the data, which extends from the late northern winter to the early northern spring seasons. Additionally, the GCM optical depth

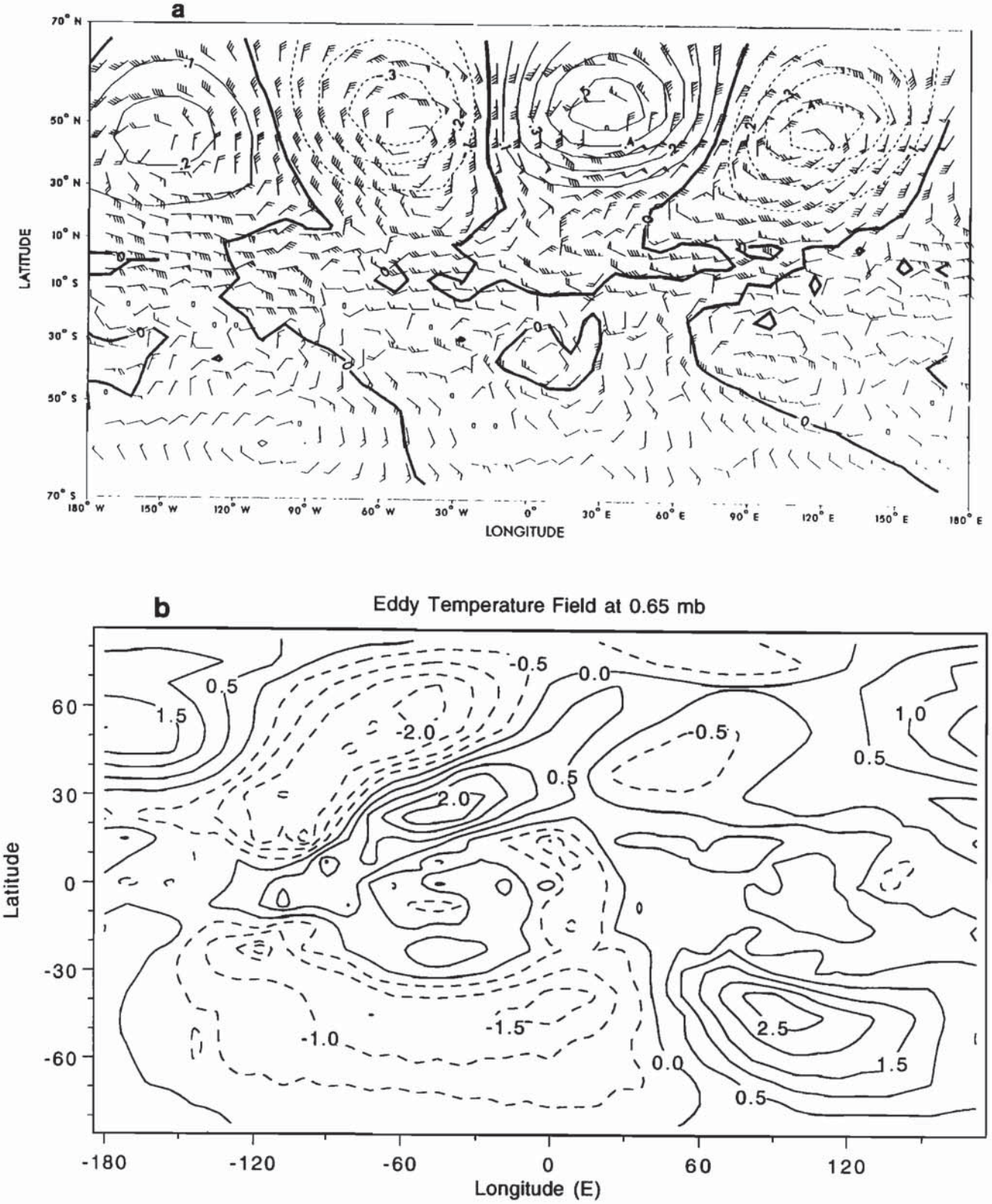

Figure 12. (a) The eddy geopotential heights and winds (as in Figure 2) at the 1-mbar level for a GCM simulation for late northern winter and a dust opacity of 0.3, and (b) the time-averaged eddy temperature field (in Kelvins) at the 0.65-mbar level from a GCM experiment centered at $L_S \sim 0°$ with a dust opacity of 0.3.

(0.3) may be somewhat off for this period of observations (and a horizontally uniform distribution of dust was surely not actually present during this period). Finally, of course, there may be very significant errors in the GCM topography. In view of all of the above, the agreement with the IRTM results can be regarded as relatively good.

4. Eddy Dynamics

4.1. Vertical and Meridional Propagation

It has been seen that the winter quasi-stationary eddies tend to exhibit their maximum geopotential and wind amplitudes at the top of the model, ~47 km-altitude. The region of largest amplitudes also tends to shift substantially poleward with increasing height. To better understand the dynamics underlying these aspects of the eddy structures, we will further examine both the mean flows and the eddies in the GCM simulations.

Figure 13 shows the geopotential amplitudes for zonal wavenumbers 1-3, for the northern winter solstice experiment with a dust opacity of 0.3. The corresponding phase structures are shown in Figure 14. It can be seen that the wavenumber 1 and 2 amplitudes are very comparable in this case, with the former increasing to the model top and the latter reaching a maximum at ~35 km. The patterns of the wave 1 and 2 amplitudes bear considerable resemblence to that of the zonal jet in this simulation [see *Barnes et al.*, 1993, Figure 1]. The wavenumber 3 amplitude displays a low-level maximum, at ~10 km, with decreasing amplitudes at higher levels; the amplitude values at upper levels (above 15-20 km) are much smaller than for waves 1 and 2. The most striking aspect of the wave phases in Figure 14 is their relative uniformity throughout the region where the wave amplitudes are sizeable: in no case is there more than about 60 degrees of phase variation in this region. This lack of phase tilt in both height and latitude was reflected in the relatively small magnitudes of the heat and momentum fluxes (see Figure 5). Such an absence of phase variation is expected for waves that are trapped in both the meridional and vertical directions.

Cross sections of the quasi-geostrophic refractive index for planetary wave propagation [e.g., *Andrews et al.*, 1987; *Palmer*, 1982] are shown in Figure 15, for wavenumbers 1-3. The distributions of refractive index would seem to be largely consistent with the wave amplitude and phase structures in Figures 13 and 14. In particular, the wavenumber 1 and 2 fields are similar, with a region of sizeable positive values extending to the model top, in the basic vicinity of the zonal-mean jet. These positive values are the result of very large values of the quasi-geostrophic gradient of potential vorticity, associated with large curvatures of the zonal winds near the jet axis. The existence of a positive "duct" in the refractive index fields for waves 1 and 2 would appear to enable a substantial vertical penetration by these eddies, with a channeling of wave energy from the subtropics and lower midlatitudes at lower levels to higher latitudes at upper levels. The refractive index pattern may indicate the presence of a relatively effective "cavity" for trapping the forced planetary wave energy, there being little net propagation in either latitude or height (as is evidenced by the wave phases in Figure 14). It can be seen that the wave 3 refractive index duct is much narrower than that for waves 1 and 2, and cuts off at higher levels. In addition, the refractive index values decrease fairly strongly with height in the duct, unlike those for waves 1 and 2. These features would seem to largely explain why wavenumber 3 appears to be strongly trapped at relatively low levels (see Figure 13).

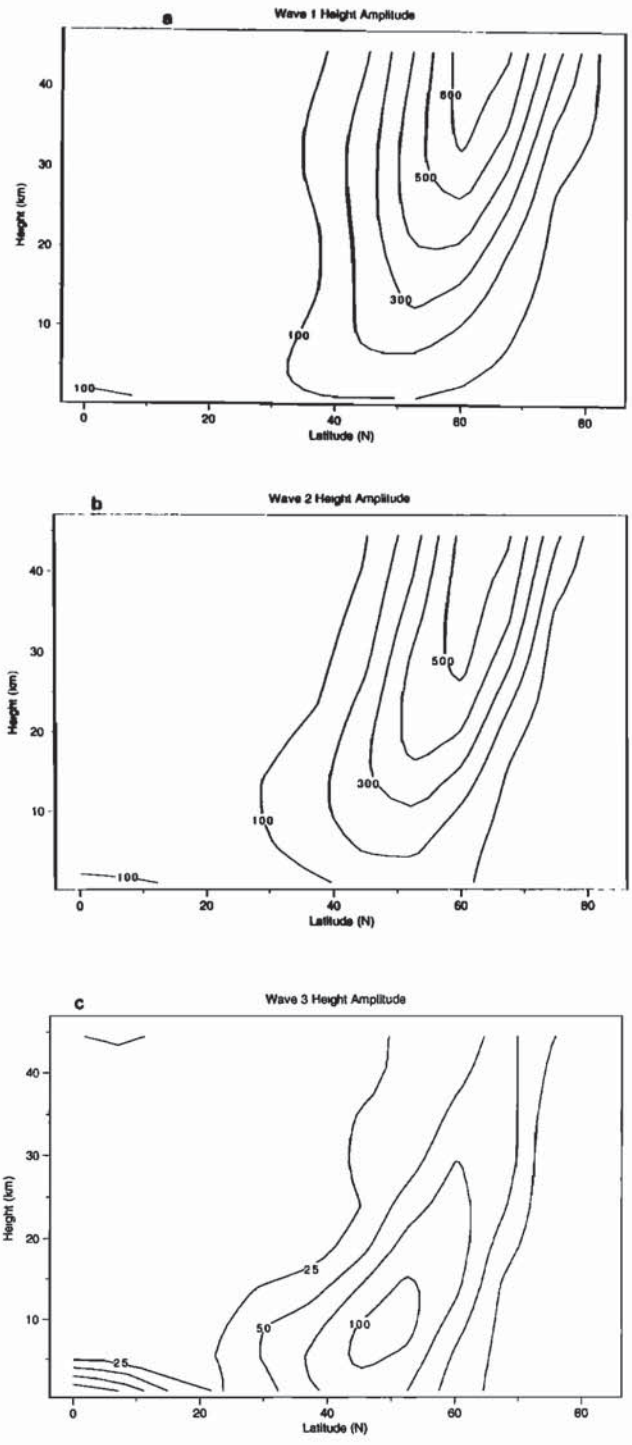

Figure 13. Latitude-height cross sections of the amplitudes (meters) of the zonal wavenumber (a) 1 , (b) 2, and (c) 3 components of the eddy geopotential height field, for the northern winter simulation with dust optical depth 0.3.

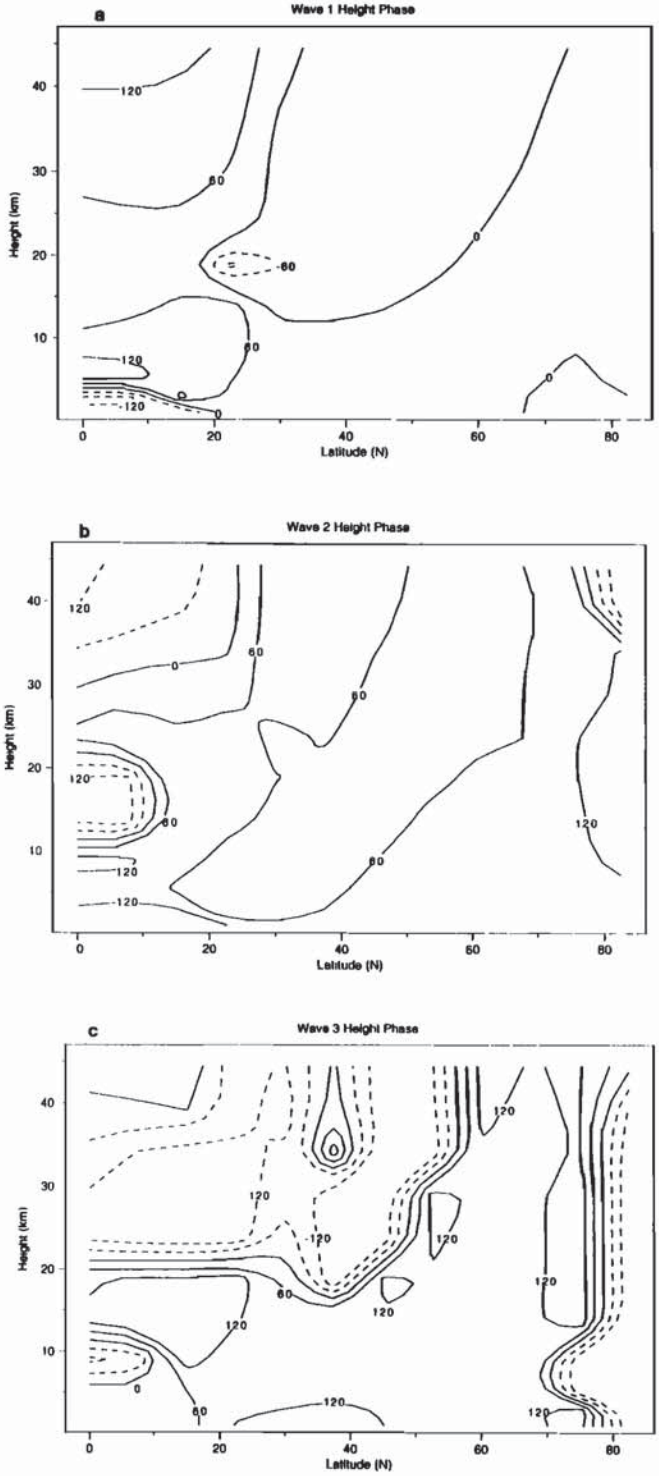

Figure 14. As in Figure 13, but for the relative wave phases (in degrees) for waves 1-3.

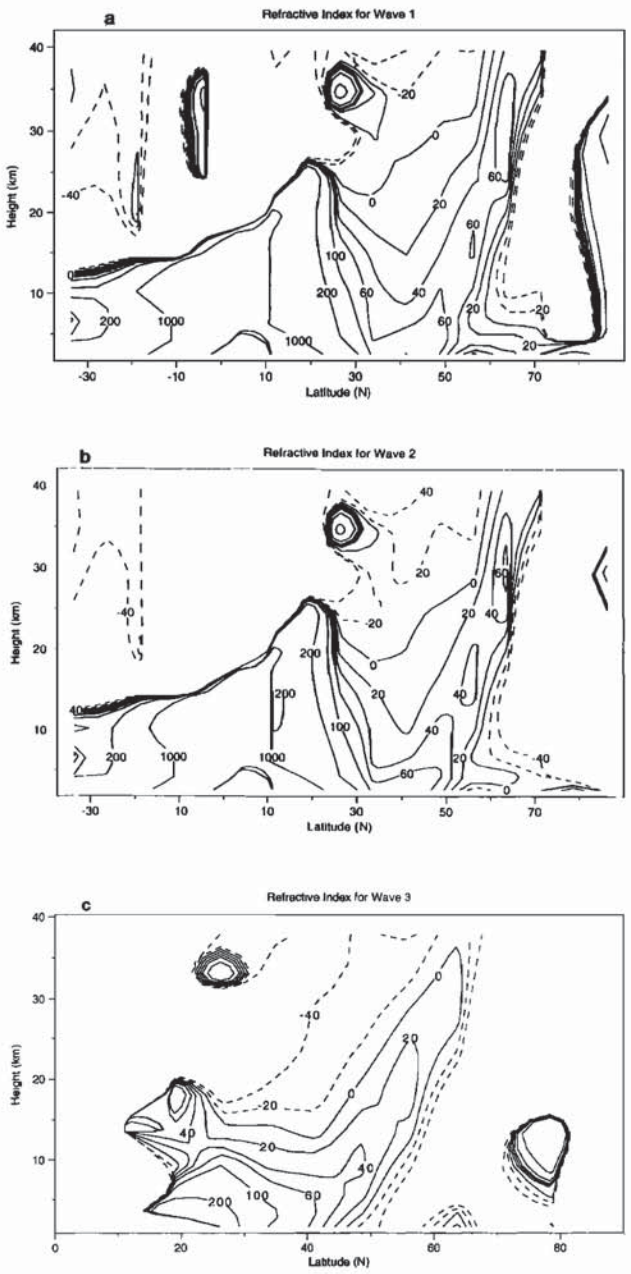

Figure 15. As in Figure 13, but for the refractive index squared, for zonal wavenumbers 1-3. The refractive index values are computed as in the work by *Palmer* [1982], and are nondimensional. Note that the contour levels are nonuniform above 60, and values less than -40 and larger than 200 have not been contoured.

For the southern winter solstice simulation which exhibits a very large amplitude wavenumber 1 disturbance, the zonal-mean jet is characterized by patterns of the refractive index (not shown) which are basically similar to those in Figure 15. The wave 1 and 2 fields would seem to be consistent with extensive vertical penetration of both waves, but wave 1 displays a very strong increase with height (a substantially greater increase than in the northern winter case) while wavenumber 2 increases only rather weakly with height, as shown in Figure 16. The wavenumber 3 amplitude distribution is quite similar to that for the northern winter simulation (see Figure 13). The basic difference between the amplitudes of waves 1 and 2 at lower levels would appear to be understandable in terms of the differences in the topographic amplitudes: the wave 1 topographic amplitude in the 30°-60°

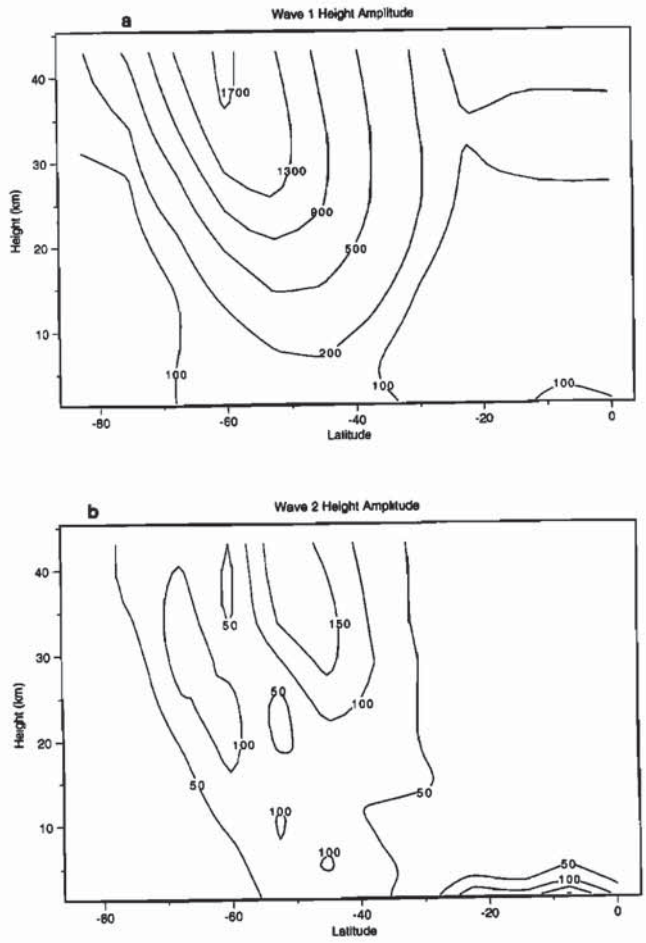

Figure 16. As in Figure. 13 but for waves (a) 1 and (b) 2, for the southern winter solstice simulation with optical depth 0.3.

S region is roughly twice as large as that for wave 2 (and much larger than the wave 1 topography in midlatitudes in the northern hemisphere). An experiment for northern winter solstice, in which the hemispheric topographies are reversed (the southern topography is placed at northern latitudes, and vice versa), yields a very large amplitude wave 1 pattern in northern middle and high latitudes. Conversely, an experiment for southern winter with a reversed topography field (the northern topography in the south) yields a strong wave 2 pattern. Interestingly, in this experiment the wave amplitudes in the western hemisphere are much larger than in the corresponding northern winter simulation (as shown in Figure 2). This would seem to point to the role of the zonal mean flow and thermal forcing (the albedo and thermal inertia fields are not reversed in the reversed topography experiments) in contributing to the west-east asymmetry in the nondusty northern winter simulation.

The reasons why the wave 1 amplitude increases so rapidly with height in the southern winter simulation and the wave 2 amplitude increases only weakly with height, in contrast to the wave 1 and 2 behavior in the northern winter case, are not clear. It appears that relatively subtle differences in the mean zonal flows may be chiefly responsible. This is indicated by the fact that the increase of the wave 2 component with height in the northern winter experiment with hemispherically reversed topography is much greater than in the southern winter case.

It can be noted that rather similar wave structures to those in the Mars GCM have been found in a three-dimensional (3D) linearized model forced by purely zonal flow over topography [*Hollingsworth and Barnes*, 1996]. In particular, large-amplitude wave 1 and 2 disturbances are obtained in the linear calculations, with wave 1 dominating strongly for the southern hemisphere topography. Both the wave 1 and 2 amplitudes increase upward from low levels to ~40-50 km; the wave 1 amplitudes continue to increase to substantially higher levels (the model top in the linear calculations is located above 100 km). These linear model results help to give some confidence that the lower model top (~45 km) in the GCM is not severely distorting the standing eddy structure. Additional linear calculations with a more simplified model (a quasi-geostrophic, beta-plane channel, model) have been performed by the lead author to try to assess the effects of the upper boundary in the GCM. These show that the results for a radiation upper boundary condition (which allows wave energy to propagate away to infinity) are not substantially different from those for the GCM "rigid-lid" (vanishing vertical velocity) upper boundary condition. This would seem to be understandable in the basic context of the waves being vertically trapped (though the amplitudes still increase with height) and not vertically propagating, as indicated by the smallness of the vertical phase tilts. The amount of wave energy reaching the upper boundary (and being reflected) is simply not large enough to have any sizeable effects upon the wave field at lower levels.

The early northern fall and late northern winter GCM simulations yield wavenumber amplitude and phase structures rather similar to those in Figures 13 and 14, with both waves 1 and 2 increasing substantially with height. The refractive index fields are also very similar to those in Figure 15 for winter solstice, so that these structures seem to be consistent. The southern winter solstice case thus stands out in having a relatively weak wavenumber 2 circulation, particularly at higher levels. The relative smallness of the wave 2 topographic forcing in the southern hemisphere was noted above, but this forcing is still comparable to that in the subtropics and midlatitudes of the north. It does appear that thermal forcing from tropical latitudes (having a strong wave 2 component) may play a more important role in northern winter than in southern winter; this is examined in the following section.

4.2. Wave Forcing

A basic issue in relation to the quasi-stationary circulations in the Mars GCM simulations is the role of mechanical versus thermal processes in their forcing. The presence of large low-level wave amplitudes in the tropics in the northern winter simulations has been noted (see Figure 4). These certainly are suggestive as to a possible important role for thermal forcing, as the near-surface zonal winds are relatively weak in this region [see *Haberle et al.*, 1993].

Mechanical forcing. On the basis of the orientations (and magnitude) of the topography and the low-level flow in the extratropics, mechanical forcing of the standing eddies in the GCM simulations should be relatively strong. Figure 17 shows the time-mean winds in the lowest model layer (at a height of ~250 m), for the nondusty northern

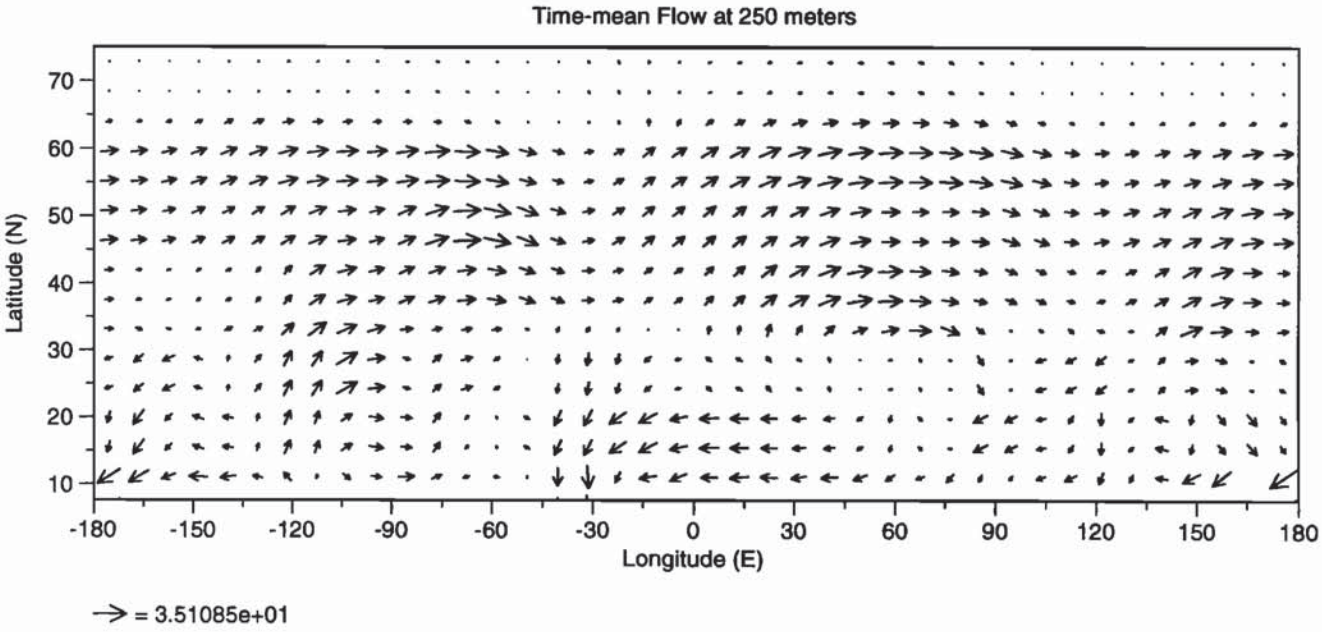

Figure 17. Time-averaged horizontal winds at the lowest GCM sigma level (~250 m), from the simulation for northern winter solstice with an optical depth of 0.3. Equal zonal and meridional wind components correspond to a vector at an angle of 45° to the horizontal map axis.

winter simulation examined above. It can be seen that there is a substantial zonal flow in middle latitudes, with peak winds of almost 30 m/s. The near-surface flow is particularly strong in the vicinity of the elevated regions, where topographic gradients are steep, and appears to be directed largely up and over the topography (and not diverted around it).

Much of the structure of the GCM standing eddies in middle latitudes appears to be consistent with that expected for mechanical forcing. In particular, the low-level structure tends to be such that the primary thermal balance is between adiabatic warming/cooling produced by the flow over the topography, and meridional temperature advection in the presence of very strong zonal-mean baroclinicity [see *Haberle et al.*, 1993 ; *Barnes et al.*, 1993]. This is illustrated in Figure 18, which shows the eddy meridional winds at the lowest model level for the nondusty northern winter simulation. It can be seen that regions of northerly/southerly flow largely coincide with areas of eastward facing/westward facing slopes, where there should be strong sinking/rising motions; the pressure ridges and troughs are essentially in phase with the topography. There is an analogous relationship between the near-surface meridional wind and topography in the southern winter simulations. The exception to this basic structure is for zonal wavenumber 1, as the wave 1 pressure pattern is shifted well to the west of the wave 1 topography in middle latitudes in the simulations with low and moderate dustiness. In this case, zonal advection of temperature must be playing a much larger role in balancing the topographically-induced adiabatic warming and cooling.

The structure of the wave 2 patterns (the geopotential/pressure being in phase with the topography) is as expected, on the basis of simple linear theory, for mechanically forced waves which are shorter than the resonant scale [*Held*, 1983]. The westward-shifted wave 1 patterns are consistent with the behavior expected for longer waves, waves longer than the resonant scale. If wave 1 is not too much longer than this scale, in the simple models, then it will still remain vertically trapped like the shorter waves. This behavior would be consistent with the GCM eddy structures.

The strong east-west asymmetry in the eddy field that is present in the nominal (low dust northern winter solstice) case indicates that wave interference effects are of importance. Tharsis should provide the forcing for a large-amplitude ridge centered near 90°-120° W, but only a very weak ridge is present in this region (see Figures 2 and 3). As discussed by *Hollingsworth and Barnes* [1996], global wave interference effects appear to be important in the Mars atmosphere because of very fast zonal group velocities for the stationary eddies. The Tharsis topography, and the other major topographic features, force a range of zonal wavenumbers (1-4, most strongly), and the propagation of these around the planet can lead to destructive interference in some regions and constructive interference in others. Simple barotropic calculations show a strong east-west asymmetry much like that obtained in the nominal experiment here, but the asymmetry is considerably less pronounced in the global baroclinic model results [*Hollingsworth and Barnes*, 1996]. The latter model yields a wave field that more closely resembles that found here in the moderately dusty (unit opacity) northern winter solstice and the late northern winter and spring equinox experiments (see Figures 6 and 12). Why these other GCM simulations exhibit much less east-west asymmetry is an open question, but differences in the zonal flow structures could be at least partly responsible. Another possibility is that the effects of thermal forcing are important in producing the east-west asymmetry: the results of the hemispherically reversed topography experiments suggest that this may be the case, as noted previously.

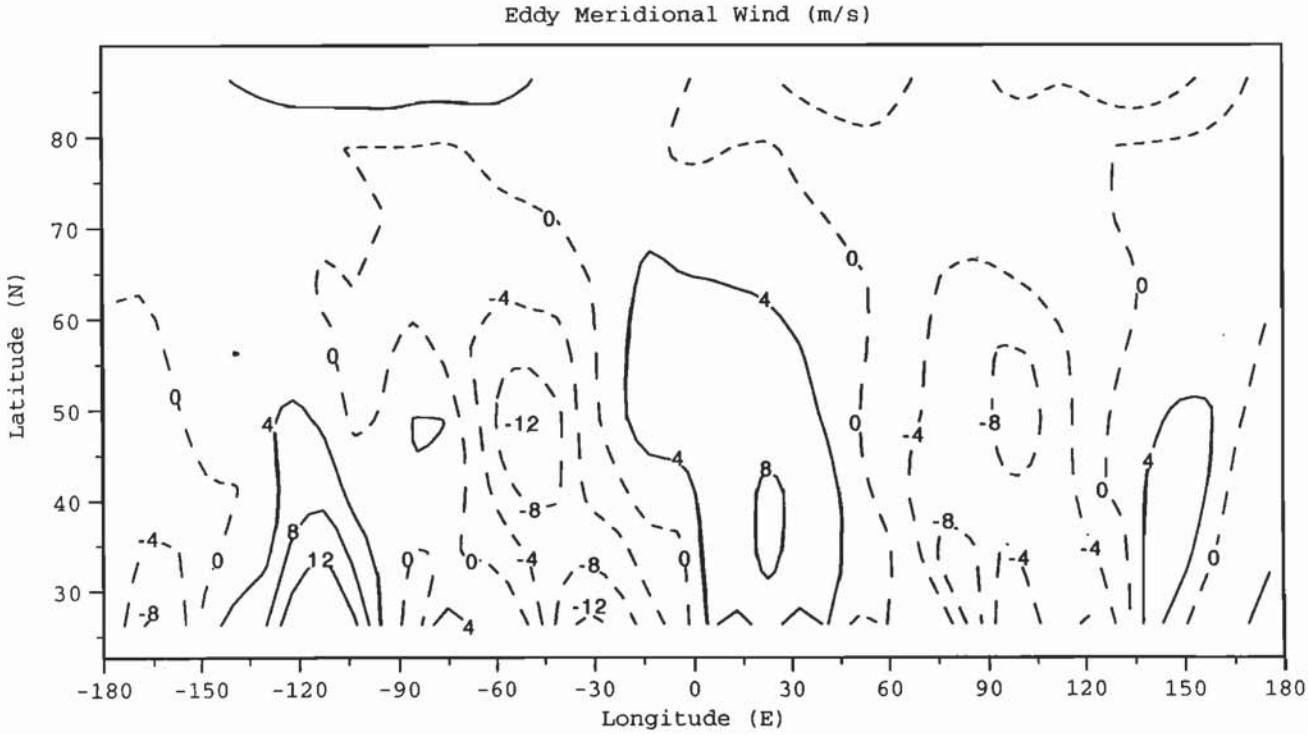

Figure 18. The time-averaged eddy meridional wind at the lowest GCM sigma level (~250 m), from the same simulation as in Figure 17.

Thermal forcing and low-latitude structure. At relatively low levels the GCM stationary eddies have substantial amplitudes in low latitudes, as can be seen in Figures 4 and 6. Figure 19 illustrates addditional aspects of the low-latitude eddy structure from two different simulations, one for northern winter solstice and a heavy dust loading (an opacity of 2.5) and the other for late northern winter and low dustiness (opacity 0.3). In the dusty winter simulation, the eddy structure in northern middle and high latitudes appears to extend into the tropics and the southern subtropical region. The eddy structures in the late winter case do not exhibit nearly as much of a low-latitude extension, except perhaps in the region on the eastern side of the Tharsis plateau. Recent linear modeling results, with purely mechanical forcing, do not show the existence of any sizeable eddy amplitudes in the tropics and the summer subtropics [*Hollingsworth and Barnes*, 1996]. The presence of these in the Mars GCM must be associated with the effects of thermal forcing and/or the existence of much stronger eddy forcing in the summer subtropical region. In the dusty winter simulations, the summer subtropical jet [see *Haberle et al.*, 1993] becomes very intense and has vigorous eddy circulations associated with it; these features are largely absent in the late winter season. The basic states used in the linear modeling studies provide no representation of the summer subtropical jet, nor of the cross-equatorial Hadley circulation which becomes very strong in the dusty winter solstice simulations. However, the fact that the linear results in the winter extratropics are in fairly good basic agreement with those from the GCM experiments would certainly seem to indicate that low-latitude forcings and the Hadley circulation are not factors of primary importance for the winter stationary eddies, except in lower latitudes.

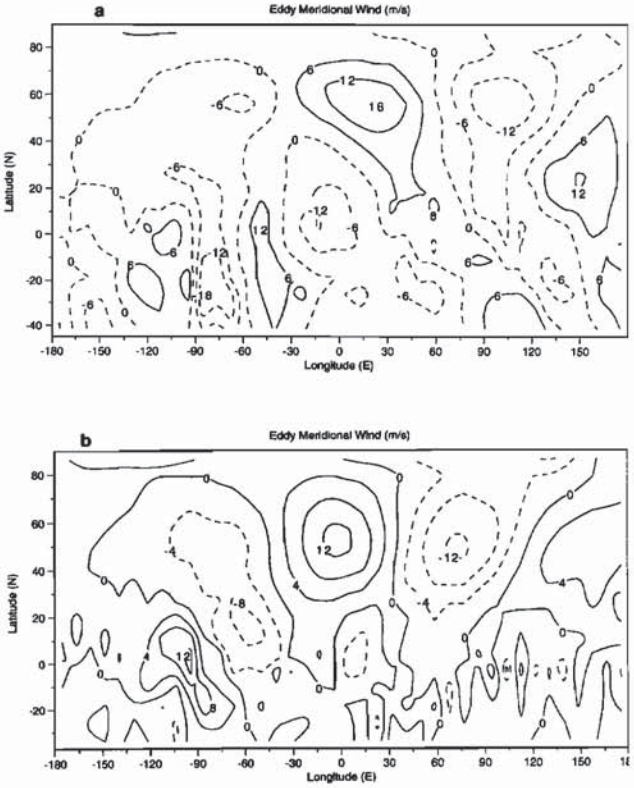

Figure 19. (a) The time-averaged eddy meridional wind component (m/s) at the ~1.8-mbar pressure level from the northern winter simulation with a dust opacity of 2.5, and (b) the same for the late northern winter simulation with optical depth 0.3.

Figure 20 shows a latitude-height cross section of Eliassen-Palm (EP) fluxes and divergences for the highly dusty northern winter experiment. It can be seen that the fluxes appear to provide evidence for the existence of near-surface forcing in the northern tropics, and propagation poleward and upward into the vicinity of the westerly zonal jet in middle and high latitudes. In addition, there appears to be propagation of wave activity from the southern hemisphere, across the equator and into northern latitudes. The northwest-southeast tilt of the disturbances in Figure 19 (most evident in the eastern hemisphere) is consistent with this, as it implies southward/northward momentum/EP fluxes. It can be noted that the magnitude of the EP flux convergence (zonal flow deceleration) at upper levels and high northern latitudes in Figure 20 is quite substantial, being in excess of 35 m/s/d.

The EP flux cross section for the late northern winter simulation (not shown) shows much less northward propagating wave activity in lower latitudes, and a relatively stronger flux of wave activity upward from low levels in northern midlatitudes. This supports the thesis that low-latitude forcing and/or thermal effects are of much greater importance in the dusty northern winter solstice simulation. The nondusty (opacity 0.3) northern winter EP cross section exhibits some of the same features as in Figure 20, but the strength of the fluxes from the tropics and the southern hemisphere is not nearly as large. In the southern winter solstice simulation, there is not much indication of the propagation of wave activity out of tropical regions. This would seem to be consistent with the relatively small eddy amplitudes outside of the southern extratropics in this case (see Figure 9).

There is relatively large zonally asymmetric diabatic heating in the tropical regions in the solstice GCM simulations. The time-averaged eddy diabatic heating field from the nondusty northern winter solstice simulation, at the ~2.8- mbar pressure level, is shown in Figure 21. It can be seen that there are maxima in the heating centered near the equator and in the tropics to the south; the most prominent feature is a region of strong heating (over 20 K/d) that essentially coincides with the Tharsis "bulge." There is a tendency for the heating regions to correspond to uplands and the regions of cooling to be located over lowlands, as might be expected given the very strong influence of the surface on atmospheric temperatures [e.g., *Webster*, 1977]. However, the pattern of heating in Figure 21 is clearly not simply explained by the topography alone. The heating and cooling features in Figure 21 are relatively shallow, being largely confined within ~10 km of the surface; the heating maximum in the Tharsis region extends to substantially lower pressure levels than the other features but is still replaced by cooling at upper levels.

The heating and cooling patterns near the surface are quite different from those in Figure 21, as can be seen in Figure 22. At very low levels, there tends to be heating in the low-lying regions and cooling in the elevated areas. The area of

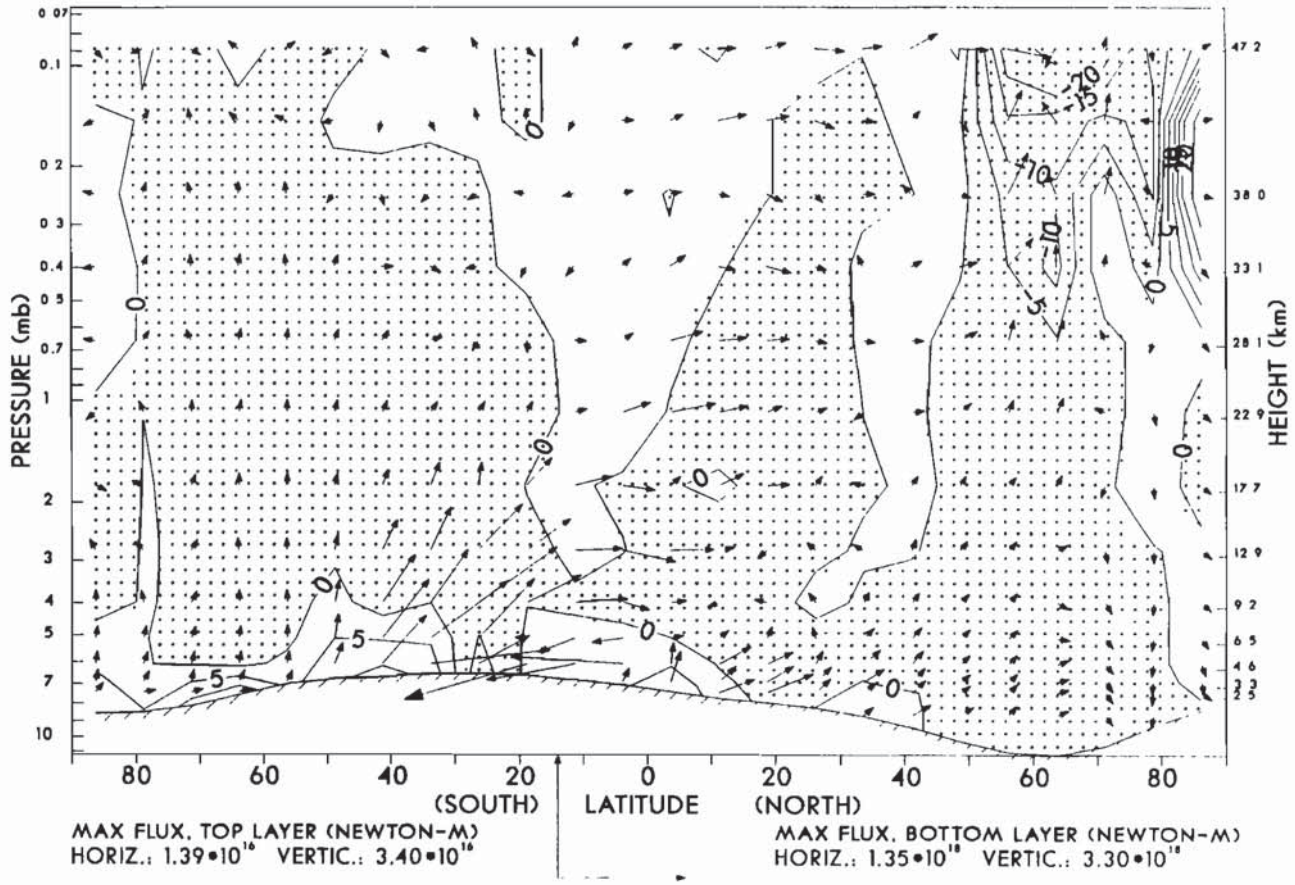

Figure 20. A time-mean Eliassen-Palm cross section for the northern winter simulation with a dust optical depth of 2.5. The EP fluxes and flux divergences have been computed using the primitive equation definitions [*Andrews et al.*, 1987] and have been plotted following the conventions of *Edmon et al.* [1980], except that the flux vectors have been inversely scaled by pressure to better show the upper level activity. The flux divergences are in units of m/s/d, and negative values (regions of flux convergence) are shaded.

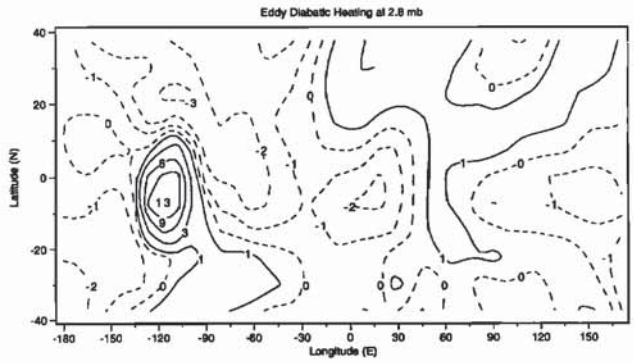

Figure 21. The time-averaged eddy diabatic heating at a pressure level of ~2.8 mbar, from the simulation for nothern winter solstice with a dust optical depth of 0.3. The heating is in units of K/d, and dashed contours correspond to net cooling.

very strong heating near 40 W is associated with quite cold temperatures near the surface, which appear to be associated with strong northerly flow along the western side of the Chryse basin, a western boundary current, which can be seen in Figure 17. Generally, the areas of heating in Figure 22 correspond to cold temperatures, and the areas of cooling to warm temperatures (see Figure 6b).

A basic issue of interest is to what extent the variable surface thermal inertia and albedo fields in the GCM may be contributing to the thermal forcing of the standing eddy circulations. The analysis of a GCM sensitivity experiment with flat topography but variable inertia and albedo (the experiment is otherwise identical to the northern winter moderately dusty case) helps to answer this. This simulation does exhibit significant time-averaged eddy circulations, as depicted in Figure 23. It can be seen in Figure 23 that there is a wave 2 pattern in winter middle and high latitudes; this pattern remains similar at lower and higher levels. Both the thermal inertia and albedo fields have strong wavenumber 2 components in northern low and middle latitudes [see *Pollack et al.*, 1990]. The wave 2 disturbance in the simulation without topographic forcing is essentially 180 degrees out of phase with those in the northern winter simulations with topography. It thus appears that the effect of the thermal inertia and albedo forcing may be to reduce the overall strength of the standing eddy circulations in winter midlatitudes.

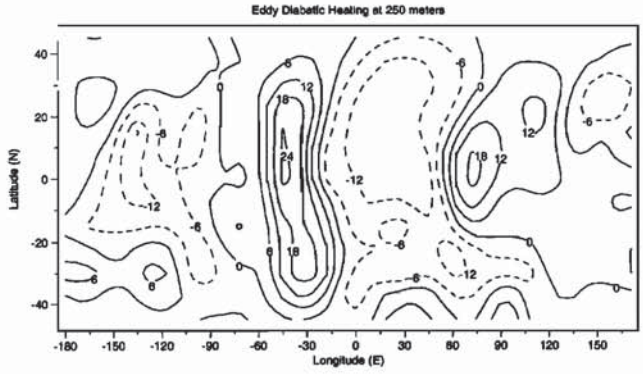

Figure 22. The time-averaged eddy diabatic heating, as in Figure 21, at the lowest GCM sigma level (~250 m).

4.3. Increases in Eddy Amplitude with Dustiness

There is a general increase in the quasi-stationary eddy amplitudes with increasing dustiness in the northern winter simulations, as noted previously. The changes with dust loading are illustrated in Figure 24, which shows a measure of the eddy amplitudes for five different solstice experiments. It can be seen that the largest wave 2 amplitude is found in the unit optical depth simulation, and the largest wave 1 amplitude occurs in the 2.5 optical depth experiment. The eddy amplitudes in the optical depth 5 case are reduced relative to these, being close to those in the optical depth 0.3 simulation.

The increase in the amplitudes of the stationary circulations with dust loading at northern winter solstice is of interest in connection with the Viking-observed polar warming during the second 1977 dust storm [e.g., *Martin and Kieffer*, 1979], and in the general context of dust-induced circulation changes. Forced stationary waves have been suggested as a mechanism that could act to produce a warming event like that seen in 1977 [*Barnes and Hollingsworth*, 1987].

There appear to be at least several possible mechanisms underlying the increase in the stationary eddy amplitudes in the Mars GCM simulations. One is an increase in the strength of the low-level forcing in the model, that due to the flow over topography as well as perhaps thermal forcing. A second is a change in the wave propagation properties of the zonal flow, produced by the sizeable changes in the zonal wind that occur as the dust loading in the GCM increases [see *Haberle et al.*, 1993]. A third possible factor is a quasi-resonant preferential amplification of the wavenumber 1 component of the stationary circulation, suggested by linear modeling [*Hollingsworth and Barnes*, 1996] and by recent dust transport experiments conducted with the Mars GCM [*Murphy et al.*, 1995].

Changes in forcing. The time-mean westerly zonal winds in northern midlatitudes in the GCM generally increase strongly with dustiness at winter solstice [*Haberle et al.*, 1993], but the near-surface winds actually decrease somewhat in strength. In the clear solstice experiment these winds are in the range of ~15-25 m/s, with a peak zonal wind of nearly 30 m/s. The peak low-level westerly wind in the optical depth 1 simulation is about 24 m/s. There is little change in the zonally averaged near-surface winds [see *Haberle et al.*, 1993; *Barnes et al.*, 1993]. The westerly flow in the optical depth 5 experiment is further reduced from that in the unit dust opacity case. It thus appears that the increases in eddy amplitudes with higher dust loadings are not due to stronger low-level mechanical forcing; rather, these increases seem to be occurring despite decreases in the strength of the low-level forcing in middle latitudes. As discussed above, it does appear that there is a stronger influx of wave activity from the tropics and the southern hemisphere into the northern hemisphere in the highly dusty cases. This may be at least partly responsible for the increase in the middle-and high-latitude quasi-stationary eddy amplitudes. In connection with this, it can be noted that the zonal-mean state in the highly dusty simulation has westerly winds extending across the equator at ~5-10 km (see *Haberle et al.*, [1993] for the optical depth 5 zonal winds). This aspect of the zonal-mean flow may be very important for the apparent increase in the influence of the tropical and southern hemisphere forcing, and is examined further in the following section.

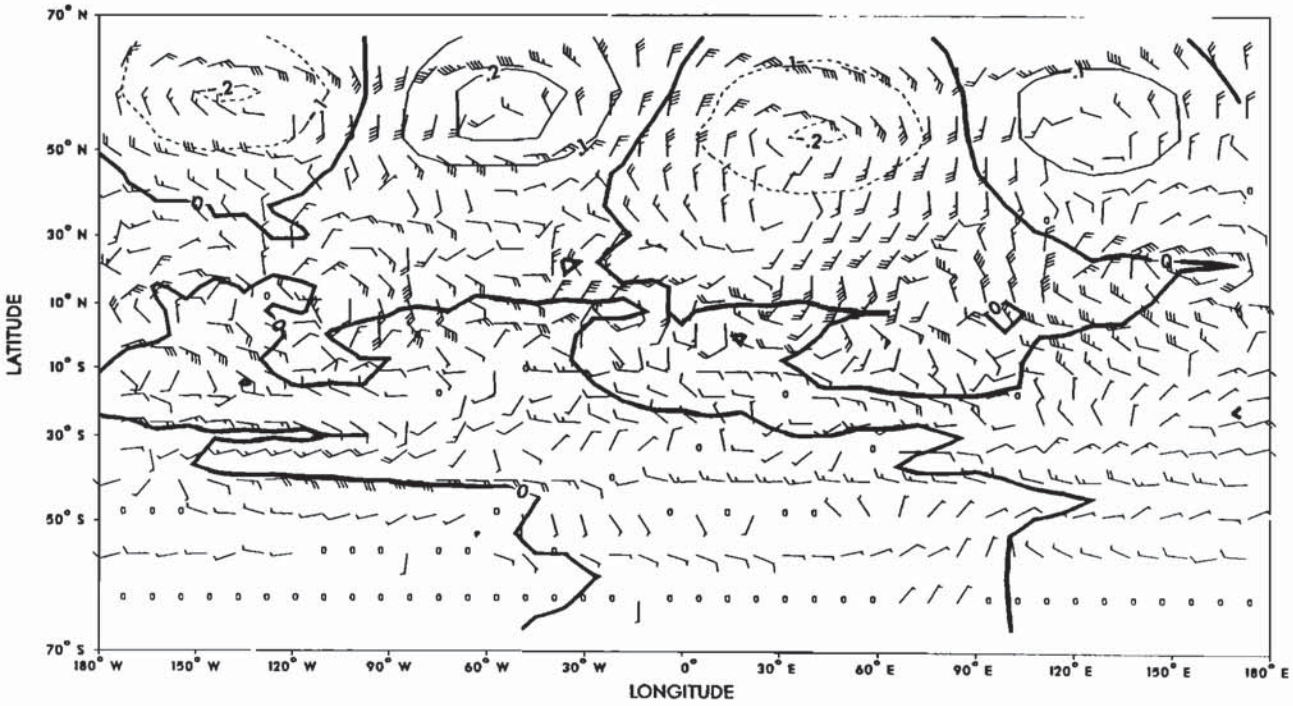

Figure 23. The eddy geopotential and wind structure at the 1-mbar level (otherwise as in Figure 2), from a northern winter solstice simulation (with dust optical depth 1) with variable albedo and thermal inertia fields but a flat topography.

Changes in propagation. The highly dusty simulation is marked by a dominant wavenumber 1 flow at upper levels. It could be that the changes in the zonal-mean flow are such as to favor the penetration of wave 1 relative to wave 2 sufficiently to yield this flow at higher altitudes With increasing dustiness, the northern winter zonal jet becomes progressively stronger, with much sharper gradients on its poleward flanks [*Haberle et al.*, 1993]. Figure 25 shows the wave 1 and 2 refractive index fields for the highly dusty (opacity 2.5) northern winter simulation, for comparison with

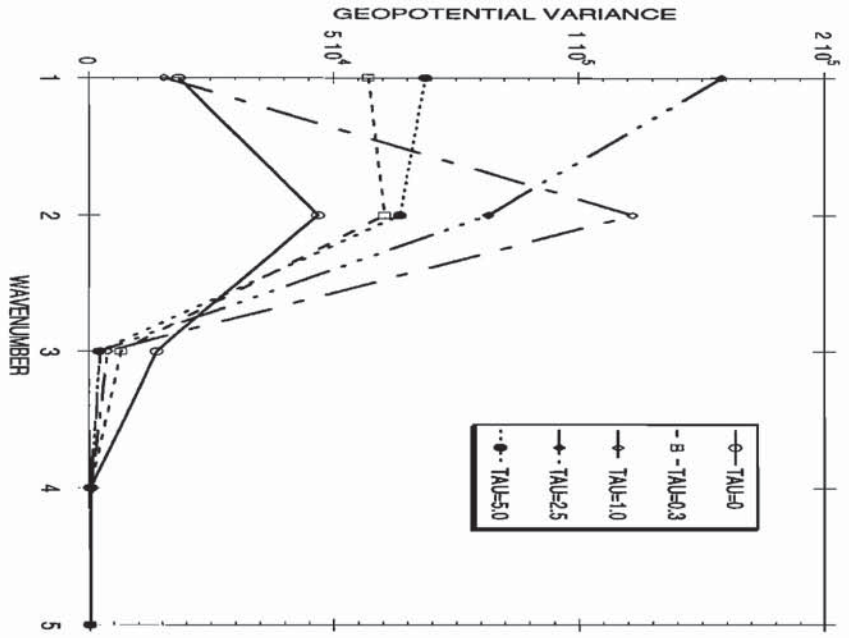

Figure 24. A measure of the stationary amplitudes of zonal wavenumbers 1-5 in the northern winter solstice simulations with varying dust loadings. The amplitude measure plotted is the geopotential variance averaged over the northern hemisphere (from 20° N to the pole, and all vertical levels without density weighting), in units of m^2.

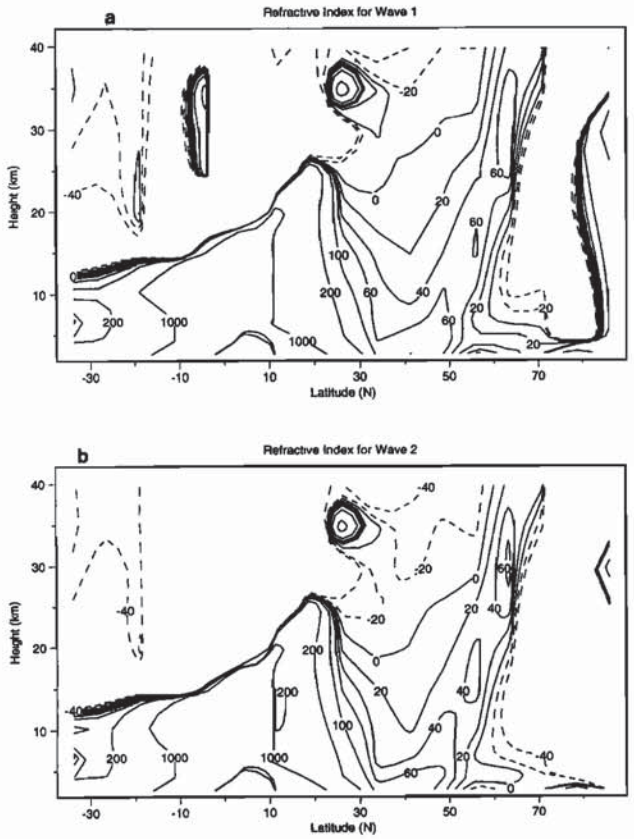

Figure 25. Refractive index fields for wavenumbers (a) 1 and (b) 2 as in Figure 15, but for the dusty northern winter simulation with an optical depth of 2.5.

those shown in Figure 15 for the nondusty (opacity 0.3) case. It can be seen that the refractive index patterns are rather similar, with one difference being that the positive values at upper levels in the "duct" are larger for both waves 1 and 2 in the dusty case. These dusty patterns could be consistent with an enhanced vertical penetration for both waves 1 and 2, and this would be consistent with the fact that the wave 1 and 2 amplitudes are both increased at upper levels in the highly dusty simulation. The wave 1 amplitude increases much more strongly than wave 2, roughly doubling in comparison to the nondusty case. This fact does not seem to be understandable in terms of the refractive index fields; any changes that are helping to produce the wave 1 dominance must be fairly subtle ones.

With even higher dust loading (an opacity of 5), the changes in the wave 1 and 2 amplitudes are not at all understandable in terms of the changes in the refractive index fields. Both the wave amplitudes decrease significantly in comparison to the optical depth 2.5 simulation, with wave 1 becoming less dominant relative to wave 2. The refractive index patterns are similar to those in Figure 25, with the upper level positive values being even greater and the meridional width of the positive duct increasing significantly. These changes would certainly seem to favor greater vertical penetration for both waves 1 and 2, but this is apparently not occurring in the extremely dusty experiment. Thus it seems difficult to explain the changes in the stationary eddy amplitudes with increasing dustiness in terms of changes in the vertical wave propagation and penetration. The zonal jet appears to become increasingly more conducive to vertical wave propagation/penetration as it becomes more intense at higher dust loadings, but the changes in the eddy amplitudes do not simply reflect this.

It can be seen in Figure 25 that the refractive index field in lower latitudes in the highly dusty simulation is very different than it is for the nondusty case (see Figure 15). In particular, positive values extend all the way to the equator at ~ 5-15 km, instead of being replaced by negative values equatorward of 15°-20° N. This pattern would indeed appear to be much more favorable for the propagation of wave activity out of the northern tropics and across the equator from the southern hemisphere. In the extremely dusty simulation with optical depth 5 the low-latitude pattern is similar, though the positive index values do not extend as far equatorward at near-surface levels.

Resonant amplification. A third mechanism that may be playing a role in the changes in the quasi-stationary eddy amplitudes with increasing dustiness is a preferential or "resonant" amplification of the wavenumber 1 component. Calculations with a linearized global circulation model indicate that changes in the basic state flow like those which occur in the dusty GCM simulations (a stronger zonal jet shifted to higher latitudes) are conducive to greatly enhanced wave 1 responses to stationary mechanical forcing [*Hollingsworth and Barnes*, 1996]. In the framework of simplified linear models, this appears to be consistent with a shift in the resonant wavenumber to smaller values, closer to 1, as the latitude of the jet and the eddies increase and the speed of the jet amplifies. In particular, in a baroclinic quasi-geostrophic β-plane channel model, with constant zonal wind $\bar{u}$, the stationary resonance is defined by

$$K_s^2 = k^2 + l^2 = \frac{\bar{q}_y}{\bar{u}} = \frac{\beta}{\bar{u}}$$

[e.g., *Held*, 1983], where k and l are the zonal and meridional wavenumbers of the perturbation and $\bar{q}_y$ is the zonal-mean potential vorticity gradient. In terms of the planetary zonal wavenumber m, this yields

$$m_s^2 = \frac{2\Omega a \cos^3\phi}{\bar{u}}$$

where l has been set to zero. For nominal parameter values for Mars ($\bar{u}$ ~ 60 m/s, ϕ ~ 50°) the above yields a relatively small wavenumber for resonance, m_s ~ 1.5. The resonant wavenumber is very strongly latitude-dependent, as well as being sensitive to the zonal flow. It is also, of course, sensitive to the meridional wavenumber, being sharply reduced for reasonable nonzero values. In a more realistic model, however, this effect of a finite meridional scale can be offset by a strong increase in the appropriate value of the potential vorticity gradient ($\bar{q}_y$) due to the meridional curvature of the mean flow. As noted earlier, the GCM winter zonal flows are characterized by very large values of the potential vorticity gradient, produced by the large meridional curvatures of the zonal winds near the jet axis.

Figure 26 shows results from calculations with a baroclinic channel model that incorporates these basic effects of finite meridional scale, by assuming a simple sinusoidal jet

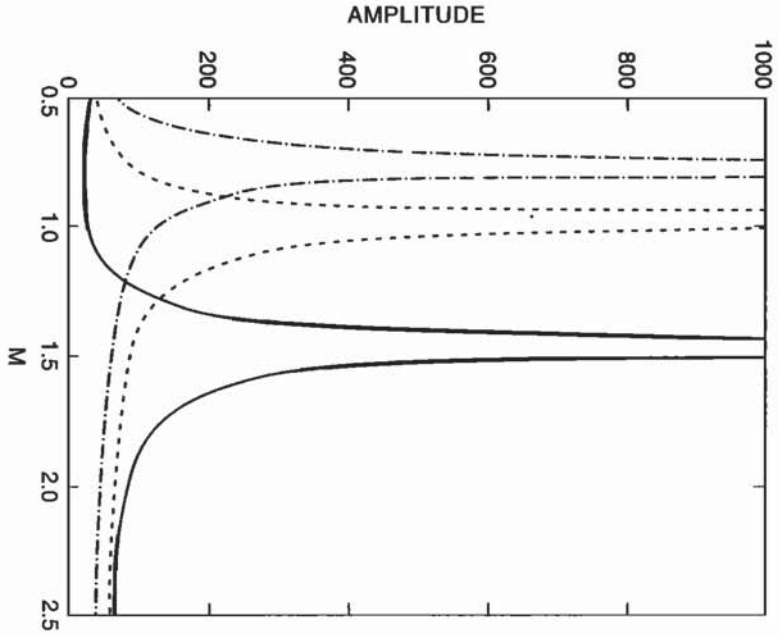

Figure 26. Wave amplitudes (in meters) at the surface as a function of zonal wavenumber for three choices of central latitude (the solid curve is for 50°, the dashed curve is for 60°, and the dashed-dot curve is for 65°) in a quasi-geostrophic beta-plane channel model. The calculations incorporate a constant Newtonian cooling with a timescale of 3 days, and an Ekman pumping with a mixing coefficient of 3 m^2/s.

profile (as in the work by *Barnes and Hollingsworth* [1987]). The zonal flow has been taken to be strongly height-dependent, with a vertical profile intended to be representative of the GCM winter flows. The calculations show a very strong dependence of the response upon latitude, with the resonant zonal wavenumber being close to 1 for a jet located at 60°. There is also a dependence upon the vertical zonal wind profile and speed in this simplified model, but it is not nearly as strong as the latitude dependence (over a range of relevant speeds).

The very substantial differences in the phases of the wave 1 disturbances between the relatively nondusty and the highly dusty GCM experiments lend support to the idea that there may be a "resonant" enhancement of wave 1 in the dusty cases. In the context of simplified linear models, the phase differences are qualitatively consistent with those expected if the resonant zonal wavenumber was significantly larger than 1 in the clear and optical depth 0.3 simulations, and somewhat smaller than 1 in the optical depth 2.5 and 5 experiments. In the former cases the wave 1 disturbance is shifted substantially to the west of the topography, whereas in the latter cases it is close to being in phase with the topography. The decrease in the wave 1 (and wave 2) amplitude in the simulation with an opacity of 5 also is potentially understandable within such a framework as a consequence of the "resonant" wavenumber continuing to decrease with dustiness (so that wave 1 lies further from it).

In the global models, where the zonal flow structure is relatively complex, an enhanced trapping of the stationary waves in the region of the jet (the formation of an enhanced wave "cavity" in middle and high latitudes) is probably a key factor in the amplification of the wave 1 response [*Hollingsworth and Barnes*, 1996]. The two-dimensional propagation of forced waves in the global models and their interaction with critical surfaces is crucial in allowing strongly enhanced or "resonant" responses to stationary forcing to occur. The linear global modeling results appear to indicate that the structure of zonal flows like those in the dusty GCM simulations is such as to allow greatly enhanced responses, even in the presence of quite strong dissipation [*Hollingsworth and Barnes*, 1996].

An additional modeling result of significance for the role of dust-induced changes in the mean flow is that experiments with a version of the Mars GCM which is coupled to a dust transport model exhibit an explosive growth in a nearly stationary wave 1 disturbance [*Murphy et al.*, 1995]. This wave 1 disturbance appears to be responsible for producing a highly transient polar warming, though it is of relatively small magnitude. In these dust storm simulations the quasi-stationary circulation changes from a wave 2 pattern to a dominantly wave 1 flow very rapidly as the northern winter zonal-mean flow "spins up" (the zonal jet intensifying and shifting poleward) in response to a rapidly increasing dust loading. Relatively enormous wave amplitudes are reached in some of these experiments, with height perturbations exceeding 4 km at upper levels. As the dust loading continues to build up, the wave 1 component begins to decay, and eventually it returns to a relatively small amplitude.

The absence of a large wave 1 disturbance in the optical depth 1 winter simulation would not appear to fit the scenario outlined above. In this regard, it can be noted that there is actually a very slowly moving (to the east), large-amplitude wave 1 disturbance present during most of this simulation. This disturbance is characterized by approximately one phase during much of the first portion of the 30-day period analyzed and a second phase that is roughly 180° different during a good

deal of the latter portion. (Space-time spectral analysis of the 30 days of data yields an eastward-propagating wave 1 period in the range of ~11-32 days, with significant power also present at very long westward propagating periods.) The time-average for the full 30-day period is then characterized by a small wave 1 amplitude, as shown in Figure 24, though the wave 2 amplitude is the largest of all the northern winter cases. The moderately dusty winter solstice case thus does exhibit a very large amplitude wavenumber 1 circulation, but one that is slowly changing and propagating and not stationary over the 30-day period.

That the zonal-mean flows in the dusty northern winter simulations may be especially conducive to slowly moving/nearly stationary wavenumber 1 disturbances is also evidenced by an optical depth 1 simulation with flat topography and uniform thermal inertia and albedo fields. A very slowly moving wave 1 component is present in this simulation without any zonally asymmetric time-averaged forcing, and the 30-day average yields significant wave 1 amplitudes: the stationary rms height variance peaks at ~300 m at upper levels. The heat and momentum fluxes for the time-averaged circulation are extremely small in comparison to the transient eddy fluxes, though, indicating a rather different eddy structure. This wave 1 disturbance could thus be a very slowly moving "free mode" (in the presence of strong dissipation), which has been excited by relatively small and random forcings. The slowly moving disturbance in the unit optical depth experiment with topography might be this same free mode in the presence of much stronger forcing (produced by the topography).

Clearly, the relatively short period (30 days) used for analysis of most of the GCM simulations can make separating transient and "stationary" disturbances somewhat problematic. Extended period simulations present difficulties for Mars because of the very large magnitude of seasonal variations. Despite this aspect of the analyses, it is clear that most of the GCM northern winter simulations with substantial dustiness (opacities of 1 and larger) exhibit large-amplitude wavenumber 1 disturbances which are either quite slowly moving or quasi-stationary. The existence of large responses at zonal wavenumber 1 in linearized models, when the mean flow is altered to be more like that obtained in the Mars GCM under dusty conditions, provides support for the hypothesis that resonant amplification may be playing an important role in the dusty northern winter simulations. Further linear studies with dusty mean flows actually taken from the GCM simulations would certainly be of interest in testing this hypothesis.

5. Summary And Discussion

Simulations of the Mars atmospheric circulation with the NASA Ames GCM are characterized by strong quasi-stationary eddy circulations in the winter hemisphere. The associated wind and temperature perturbations generally tend to increase in amplitude with height (maximum winds are generally found at the highest model level, at ~47 km) and are largest in middle and high latitudes above ~ 5-10 km in the vicinity of the axis of the winter westerly jet. The structure of the stationary eddies is close to equivalent barotropic, as there tends to be little phase variation in height; latitudinal phase variations are also relatively small. Essential aspects of the stationary eddy circulations remain largely unchanged between simulations with the Mars Consortium and DTM topographic data sets.

The winter standing eddy circulations in the southern and northern hemispheres differ significantly in zonal structure, as a very large-amplitude wave 1 pattern is present in southern winter instead of the dominantly wave 2 pattern that is present in the northern hemisphere for low and moderate dustiness. The much larger magnitude of the wave 1 topographic component in middle latitudes in the south appears to be the primary explanation for this, as the zonal-mean flows are quite similar in the two winter seasons (for the same dust loadings).

At an equinox season, $L_S \sim 0°$, the GCM produces deep quasi-stationary eddy circulations in both hemispheres, with a predominantly wave 2 pattern in the north and a wave 1 pattern in the south. A similar standing eddy field, at the ~25-km level, has recently been revealed by careful analyses of Viking IRTM data for this seasonal period [*Banfield et al.*, 1996]. The agreement of the GCM results with the observations is good for both the basic structure and the amplitude of the eddies, but sizeable phase differences are present.

The GCM winter quasi-stationary eddy circulations are dominated by zonal wavenumbers 1 and 2 at middle and upper levels. At low levels, below ~10 km, the higher wavenumbers can be more significant for the flow. The general tendency for the lowest wavenumbers to dominate the flow above low levels appears to be understandable in terms of the basic planetary wave propagation properties of the mean flows. In particular, the very strong and relatively narrow westerly winter jets appear to allow both waves 1 and 2 to propagate/penetrate to the top of the GCM, whereas wave 3 is strongly trapped at lower levels. The other aspect of the wave 1 and 2 dominance is that it appears (on the basis of simple linear theory) that the zonal flows favor an enhanced stationary response at these scales. There is, furthermore, quite substantial topographic forcing at these scales (though the wave 3 topography in middle latitudes is larger in both hemispheres) and this forcing is relatively "global" in nature. As noted by *Hollingsworth and Barnes* [1996], the topographic forcing on Mars is not nearly as "isolated" as that on Earth. Even to the extent that the forcing may be somewhat local in nature (as for, e.g., Tharsis), however, it appears that the existence of fast zonal group velocities leads to a global response [*Hollingsworth and Barnes*, 1996].

With increasing dustiness in the northern winter simulations, wave 1 becomes much more prominent. The experiment with an optical depth of 2.5 resembles the southern winter simulation, though the wave 1 forcing in the north is much smaller. Although changes in the strength of the low-level forcing and the propagation properties of the mean circulation may be of some significance for the shift from a wave 2 to a much stronger wave 1 flow, it is difficult to understand the standing eddy variations in these terms. There are good indications, as well as support from other modeling studies (including some with the GCM itself), that the GCM mean flows become much more favorable for a response to stationary wave 1 forcing with increasing dustiness. This change is associated with the considerable strengthening and poleward shift of the winter jet that takes place as the dust level rises. The fact that substantial changes in the stationary eddies may occur as the level of dust loading increases (these are especially dramatic in the dust transport experiments carried out by *Murphy et al.*, [1995] is certainly of possible

importance in relation to polar warming behavior associated with global dust storms.

The basic structure of the GCM eddies points to a primary role for mechanical forcing by the large topography. This is supported by results from linear modeling with purely mechanical forcing [*Hollingsworth and Barnes*, 1996]. Despite this, thermal forcing appears to be of significance as well, especially in the dusty simulations. The low-level standing eddy amplitudes are largest in the tropics in the simulations for northern winter, though this is not the case in the southern winter experiments. In the highly dusty simulations, disturbances at lower levels in the tropics become very prominent, and there are strong indications of the propagation of wave activity out of this region and into middle latitudes. There are also large-amplitude stationary disturbances present in the subtropics of the southern hemisphere, and it appears that there is propagation of eddy activity through the tropics and into the northern hemisphere. The refractive index structure of the dusty mean flows appears to be consistent with the existence of cross-equatorial propagation. Linear studies with basic states and diabatic heating fields like those in the GCM simulations would certainly be of interest in helping to better understand the relative roles of mechanical and thermal forcing in the quasi-stationary eddy circulations on Mars.

The GCM standing eddies have wind amplitudes that are relatively small in comparison to the very strong mean zonal flows present in the winter hemisphere. At upper levels the eddy winds do not exceed about 25-30 m/s, in regions where the mean zonal winds are mostly in excess of 100 m/s. Below ~10 km the eddy winds generally are smaller than ~10-20 m/s; the zonal flow at ~10 km exceeds ~50-80 m/s [see *Haberle et al.*, 1993]. Very close to the surface, the magnitude of the eddy winds does become comparable to that of the zonal-mean winds (see Figure 17). It thus appears that the GCM quasi-stationary eddies are fairly linear in nature, with nonlinear effects being relatively unimportant for the eddies themselves as well as the mean flows in the GCM. The apparent utility of linear diagnostics (the refractive index and the EP flux) in the interpretation of the dynamics of the GCM eddies is certainly evidence of their relatively linear nature. At low levels, however, and in connection with the forcing processes, nonlinear effects may certainly be of greater importance.

Future simulations with the NASA-Ames Mars GCM, with improved spatial resolutions (both meridional and vertical) and a higher upper boundary, will be of interest in relation to the quasi-stationary eddies. The occurrence of maximum eddy amplitudes near or at the model top (where the GCM has a "sponge layer") raises some concerns about possible distortions in the eddy structures and amplitudes. Recent studies with a linear model, however, with a top located above 100 km, yield similar structures to those found here below ~40-50 km [*Hollingsworth and Barnes*, 1996]. The geopotential and wind amplitudes in the linear model reach a maximum in the 50 to 80-km altitude region, with the actual values being very sensitive to the strength of the dissipation at these levels. GCM experiments with an upper boundary at ~80-90 km thus certainly would be desirable, for better simulations of the winter standing eddies as well as other components of the middle atmospheric circulation.

A final item of note is the significance of the winter standing eddies for landed spacecraft investigations of the Martian atmosphere. Though the regional time-mean circulations in the tropics and the southern summer subtropics appear to be considerably stronger near the surface, those in the winter extratropics (see Figure 17) could certainly produce very sizeable longitudinal differences in measured meteorological parameters. One possible example might be the time-mean zonal winds observed by the Viking Lander 2 spacecraft, which were quite light [*Barnes*, 1980, 1981]. The location of Viking Lander 2 (about 135° E and 48° N) appears to be one of relatively weaker zonal flow in the GCM simulations here, and any extrapolation to the zonal-mean is clearly problematic. The transient eddy activity in the GCM also exhibits quite strong regional variability in the winter midlatitudes and subtropics (Hollingsworth et al., 1996), and this is tied to the topography and the standing eddies. Finally, the quasi-stationary winter eddy circulations could tend to promote greater cloudiness and/or dustiness in certain regions. The western flanks of the major upland regions are areas of strong rising motion (favoring cloud formation and greater dust suspension), and also poleward winds. The latter might be expected to produce positive water vapor advection in these regions during winter, contributing further to cloud formation.

Higher resolution and improved (in model physics) GCM experiments are certainly desirable for the further study of regional variations in the Martian circulation, but greatly improved knowledge of the global/large-scale topography is absolutely critical. The latter should result from the Mars Global Surveyor laser altimeter (MOLA) experiment in 1998.

Acknowledgments. The lead author's participation in this investigation has been supported by the Planetary Atmospheres Program of NASA, and by a research contract with NASA Ames Research Center. The Planetary Atmospheres Program has provided continuing support for the Mars GCM development and studies. The authors wish to acknowledge helpful discussions and input from a number of collaborators on the GCM project, including J. Murphy, C.B. leovy, R.W. Zurek, and J.L. Hollingsworth. P.B. James and an anonymous referee provided a number of helpful suggestions and comments.

References

Andrews, D. G., J. R. Holton, and C. B. Leovy, *Middle Atmosphere Dynamics*, Academic, San Diego, Calif., 1987.

Banfield, D., A. D. Toigo, A. P. Ingersoll, and D. A. Paige, Martian weather correlation length scales, *Icarus*, in press, 1996.

Barnes, J. R., Time spectral analysis of midlatitude disturbances in the Martian atmosphere, *J. Atmos. Sci.*, *37*, 2002-2015, 1980.

Barnes, J. R., Midlatitude disturbances in the Martian atmosphere: A second Mars year, *J. Atmos. Sci.*, *38*, 225-234, 1981.

Barnes, J. R., and J. L. Hollingsworth, Dynamical modeling of a planetary wave mechanism for a Martian polar warming, *Icarus*, *71*, 313-334, 1987.

Barnes, J. R., J. B. Pollack, R. M. Haberle, C. B. Leovy, R. W. Zurek, H. Lee, and J. Schaeffer, Mars atmospheric dynamics as simulated by the NASA Ames general circulation model 2. Transient baroclinic eddies, *J. Geophys. Res.*, *98*, 3125-3148, 1993.

Conrath, B. J., Planetary-scale wave structure in the Martian atmosphere, *Icarus*, *48*, 246-255, 1981.

Edmon, H. J., B. J. Hoskins, and M. E. McIntyre, Eliassen-Palm cross-sections for the troposphere, *J. Atmos. Sci.*, *37*, 2600-2616, 1980.

Gadian, A. M., The dynamics of and the heat transfer by baroclinic eddies and large-scale stationary topographically forced long waves in the Martian atmosphere, *Icarus*, *33*, 454-465, 1978.

Greeley, R., A. Skypeck, and J. B. Pollack, Martian aeolian features and deposits: Comparisons with general circulation model results, *J. Geophys. Res.*, *98*, 3183-3196, 1993.

Haberle, R. M., J. B. Pollack, J. R. Barnes, R. W. Zurek, C. B. Leovy, J. Murphy, H. Lee, and J. Schaeffer, Mars atmospheric dynamics as simulated by the NASA Ames general circulation model, 1. The zonal-mean circulation, *J. Geophys. Res.*, *98*, 3093-3123, 1993.

Held, I. M., Stationary and quasi-stationary eddies in the extratropical troposphere: Theory, in *Large-Scale Dynamical Processes in the Atmosphere*, edited by B. Hoskins and R. Pearce, pp. 127-168, Academic Press, , San Diego, Calif., 1983.

Hollingsworth, J. L., and J. R. Barnes, Forced stationary planetary waves in Mars' winter atmosphere, *J. Atmos. Sci.*, *53*, 428-448, 1996.

Hollingsworth, J. L., R. M. Haberle, J. R. Barnes, A. F. C. Bridger, J. B. Pollack, H. Lee, and J. Schaeffer: Orographic control of storm zones on Mars, *Nature*, *380*, 413-416, 1996.

Jakosky, B. J., and T. Z. Martin, Mars: North polar atmospheric warming during dust storms, *Icarus*, *72*, 528-534, 1987.

Joshi, M. M., S. R. Lewis, P. L. Read, and D. C. Catling, Western boundary currents in the atmosphere of Mars, *Nature*, *367*, 548-551, 1994.

Joshi, M. M., S. R. Lewis, P. L. Read, and D. C. Catling, Western boundary currents in the Martian atmosphere: Numerical simulations and observational evidence, *J. Geophys. Res.*, *100*, 5485-5500, 1995.

Leovy, C. B., and Y. Mintz, Numerical simulations of the weather and climate of Mars, *J. Atmos. Sci.*, *26*, 1167-1190, 1969.

Martin, T. Z., and H. H. Kieffer, Thermal infrared properties of the Martian atmosphere, 2, The 15-μm band measurements, *J. Geophys. Res.*, *84*, 2843- 2852, 1979.

Mass, C., and C. Sagan, A numerical circulation model with topography for the Martian southern hemisphere, *J. Atmos. Sci.*, *33*, 1418-1430, 1976.

Murphy, J. R., J. B. Pollack, R. M. Haberle, C. B. Leovy, O. B. Toon, and J. Schaeffer, Three dimensional numerical simulation of Martian global dust storms, *J. Geophys. Res.*, *100,26,357-26,376* , 1995.

Palmer, T. N., Properties of the Eliassen-Palm flux for planetary scale motions, *J. Atmos. Sci.*, *39*, 992-997, 1982.

Pollack, J. B., C. B. Leovy, P. W. Greiman, and Y. Mintz, A Martian general circulation experiment with large topography, *J. Atmos. Sci.*, *38*, 3-29, 1981.

Pollack, J. B., R. M. Haberle, J. Schaeffer, and H. Lee, Simulations of the general circulation of the Martian atmosphere, 1. Polar processes, *J. Geophys. Res.*, *95*, 1447-1474, 1990.

Webster, P. J., The low-latitude circulation of Mars, *Icarus*, *30*, 626-649, 1977.

Wu, S. S. C., R. Jordan, and F. J. Schafer, Mars global topographic map 1:15,000,000 scale, *NASA Tech. Memo.*, *TM-88383*, 614-617, 1986.

Zurek, R. W., J. R. Barnes, R. M. Haberle, J. B. Pollack, J. E. Tillman, and C. B. Leovy, Dynamics of the atmosphere of Mars, in *Mars*, edited by H. H. Kieffer, B. M. Jakosky, C. W. Snyder, and M. Matthews, pp. 835-933, Univ. of Ariz. Press, Tucson, 1992.

J. R. Barnes, College of Oceanic and Atmospheric Sciences, Oregon State University, Corvallis, OR 97331 (e-mail: barnes@ats.orst.edu)

R. M. Haberle, NASA Ames Research Center, 245-3, Moffett Field, CA 94035 (e-mail: haberle@humbabe.arc.nasa.gov)

H. Lee and J. Schaeffer, Sterling Software Inc., Palo Alto, CA 94303 (e-mail: jschaef@mintz.arc.nasa.gov)

(Received May 31, 1995; revised January 8, 1996;
accepted January 16, 1996.)